

The Spread of COVID-19 in London: Network Effects and Optimal Lockdowns*

Christian Julliard †

Ran Shi ‡

Kathy Yuan §

November, 2022

Abstract

We generalise a stochastic version of the workhorse SIR (Susceptible-Infectious-Removed) epidemiological model to account for spatial dynamics generated by network interactions. Using the London metropolitan area as a salient case study, we show that commuter network externalities account for about 47% of the propagation of COVID-19. We find that the UK lockdown measure reduced total propagation by 44%, with more than one third of the effect coming from the reduction in network externalities. Counterfactual analyses suggest that: *i*) the lockdown was somehow late, but further delay would have had more extreme consequences; *ii*) a targeted lockdown of a small number of highly connected geographic regions would have been equally effective, arguably with significantly lower economic costs; *iii*) targeted lockdowns based on threshold number of cases are not effective, since they fail to account for network externalities.

Keywords: COVID-19, networks, key players, spatial modelling, SIR model.

JEL codes: I12, I18, C51, C54, D85.

*We thank seminar participants at the London School of Economics and London Business School.

†Department of Finance, FMG, and SRC, London School of Economics, and CEPR; c.julliard@lse.ac.uk

‡Department of Finance, University of Colorado Boulder, ran.shi@colorado.edu

§Department of Finance, FMG, London School of Economics, and CEPR; k.yuan@lse.ac.uk

Introduction

Facing the challenges of the COVID-19 pandemic, governments worldwide have resorted to large scale lockdown policies to contain the infectious disease. However, large scale lockdown policies have high economic costs. For example, according to the Office for National Statistics (ONS), UK gross domestic product (GDP) fell in the second quarter of 2020 – the period when the UK was in national lockdown – by 20.4% compared with the previous three months. This is the biggest quarterly decline since comparable records began in 1955. In this context, it is worthwhile to explore whether it is possible to minimise the (expected) size of infected population by optimally choosing the lockdown areas. Our estimation of the COVID-19 epidemic dynamic in London allows us to investigate whether targeted lockdowns might have achieved the same outcome, in containing the epidemic spreading, as the full-scale lockdown. Therefore, this paper aims at providing information for designing cost-minimising optimal lockdown policies conditional on epidemic effects.

To capture the COVID-19 epidemic dynamic in London, we generalise the single-population *deterministic* susceptible-infectious-recovered (SIR) model developed by [Kermack and McKendrick \(1927\)](#).¹ We incorporate *stochastic* transmission within and between the heterogeneous subpopulations of the London boroughs that are connected via the *commuting network*. Our model features multiple groups, allows disease spread dynamics in each of them to be different (*autoregressive effects*), and connects them through commuter network links (*network effects*). In short, we name it the *Network-SIR* model. We allow the model to account for potential confounding variables – the so called *endemic effects*. To quantify the impacts of lockdown policies, we parameterise the model to reflect the changes induced by the nationwide lockdown in the UK on March 23, 2020.

We estimate the model for daily COVID-19 surveillance data across 32 London boroughs. In particular, we decompose the contributing factors of the pandemic spread into three components: 1) local dynamic (intra-location) effects (people spreading the disease over time to others living in the same borough); 2) the network (inter-location) effect (people spreading the disease to other boroughs via their commute to, and interactions at, work locations); 3) the endemic effects (the confounding effects such as e.g., time fixed effects as well as borough specific characteristics and unobserved heterogeneity). Our estimation results confirm the essential role of network spillover effects via the commuting network, with existing cases in one London borough transmitting the disease to residents in other boroughs. The estimated magnitude of these network effects is large: they contribute to over 42% of all COVID-19 cases in London. In comparison, local within-borough dynamics account for less than 35% of all COVID-19 cases.

¹The core ingredients of SIR models were first formulated by Lowell Reed and Wade Frost in the 1920s, but they were not published.

According to our estimates, the March 23 nationwide lockdown (a work-from-home requirement with a small set of exceptions) is effective in containing the spread of COVID-19 cases in London. The policy reduces the number of cases generated by local transmission by around 75% of its pre-lockdown level, lowers the spillovers from workplaces to residential areas by about 12%, and decreases the home-to-work transmissions by as much as 80%.

From our estimated stochastic Network-SIR model, a tight and salient upper-bound can be computed for the so-called disease R_0 (basic reproduction number). This number represents the expected number of new cases that are *directly* infected by one existing case within a given time span (one week in our benchmark). The point estimate is around 1.4 before the nationwide lockdown, and is reduced to about 0.8 afterwards. The reduction is large, and is especially encouraging as the upper bound for R_0 drops well below one after the policy change.

To identify the pivotal boroughs for the spreading of the COVID-19 pandemic, we also derive and estimate the network impulse response functions (NIRFs) motivated by [Denbee, Julliard, Li, and Yuan \(2021\)](#). We find that the Westminster/City of London location, due to its centrality in the commuting network, dominates all other London boroughs in terms of externalities generated: before the lockdown, one additional case at this location generates (almost) three new expected cases in the whole greater London area within one week (despite Westminster/City of London ranking only 26th out of 32 boroughs in terms of total local cases before the lockdown).

Finally, we simulate alternative targeted lockdown policies based on the estimated dynamics of the Network-SIR model and the observed reduction in borough-specific activity as measured by the Google's COVID-19 Community Mobility Reports (cellphone tracking) data. The principle behind our targeted lockdown designs is simple: imposing work-from-home restrictions (of the same type as the observed ones) to fewer regions is less costly than imposing it to the totality of the city. When considering a work-from-home requirement limited to only one borough, we find that restricting workplace activity in Westminster/City of London – the borough with the largest NIRF, but very few local cases – minimises the total expected number of infected cases. This result indicates that optimal lockdowns should not only target areas with large number of cases, but also the locations in the network that are key for the COVID-19 propagation dynamics. Similarly, when constraining the optimal work-from-home restriction to two boroughs only, we find that the optimal target areas are Westminster/City of London – again, the borough with the largest NIRF – and Southwark – the borough with the highest number of cases. Therefore, optimal lockdown policies should be based on both the number of cases and the network centrality in transmitting the disease. Furthermore, our simulations suggest that a lockdown (implemented as work-from-home requirements of the same type as observed in the historical sample) of just these two boroughs would have achieved comparable outcomes, in terms of total infections in the Greater London area, as the actual national lockdown. This finding questions the optimality of the full-scale lockdown and

calls for a careful redesign of the partial lockdown policies.

Related Literature. Our paper is closely related, and contributes, to three strands of literature: the literature on covid policies targeting transmission dynamics, the literature on econometric models of covid transmission, and the network literature on both spillovers and epidemiology.

Most policy analysis of the COVID-19 pandemic in the literature focuses on the trade-off between sustaining economic output and saving lives. A starting point for this type of analysis is well-specified disease transmission dynamics – and that is exactly what we deliver. [Avery, Bossert, Clark, Ellison, and Ellison \(2020\)](#) provide an overview of various models for the spread of COVID-19. The dominant paradigm the existing literature adopts is still the Kermack-McKendrick SIR framework. Under this framework, several studies investigate the optimal testing, tracing, vaccine distribution, and lockdown policies in light of different socioeconomic costs ([Alvarez, Argente, and Lippi, 2021](#); [Eichenbaum, Rebelo, and Trabandt, 2021](#); [Farboodi, Jarosch, and Shimer, 2021](#); [Garriga, Manuelli, and Sanghi, 2022](#); [Jones, Philippon, and Venkateswaran, 2021](#)). Similar to the calibration exercises in [Farboodi et al. \(2021\)](#), our optimal policy simulations also use data from Google’s COVID-19 Community Mobility Reports. Policy prescriptions from these studies treat the whole population as homogeneous, thus, are silent on targeted lockdowns. Along the line of targeted optimal policies, our analysis is most related to [Gollier \(2020\)](#) and [Acemoglu, Chernozhukov, Werning, and Whinston \(2021\)](#). In their analysis, lockdowns target different age groups. Our policies are designed for local authorities and were implemented in the UK during the second wave of COVID-19 outbreak in 2020.

Our work also belongs to the literature on developing econometric models for the dynamics of COVID-19 transmission. Examples of univariate models for the COVID-19 contact and infection processes include [Li and Linton \(2021\)](#) and [Fernández-Villaverde and Jones \(2022\)](#), both of which estimate their models for different regions separately. In addition, [Chernozhukov, Kasahara, and Schrimpf \(2021\)](#) and [Lee, Liao, Seo, and Shin \(2021\)](#) develop methods to estimate policy impacts using graphic models and data-driven change point detection algorithms. Joint analysis of disease spread dynamics across multiple locations, such as our model, is also presented by [Liu, Moon, and Schorfheide \(2021\)](#) under a dynamic panel data setting. The findings of [Liu, Moon, and Schorfheide \(2021\)](#) confirm that borrowing information across different locations can strengthen model performance (in terms of forecasting). Different from [Liu et al. \(2021\)](#), our model 1) allows “network covariates” that capture interpretable transmissions dynamics across locations and 2) has a likelihood function that is derived based on direct implications of SIR models about disease surveillance data.

Our paper is also related to the network literature on epidemiology (see, e.g. [Newman \(2002\)](#), [Jackson \(2008, Chapter 7, Sections 7.1 and 7.2\)](#) and [Easley and Kleinberg \(2010, Chapter 21\)](#)). Our optimal lockdown policy targeting network “key players” is motivated

by Ballester, Calvó-Armengol, and Zenou (2006) and Denbee, Julliard, Li, and Yuan (2021). There is also empirical literature highlighting the importance of network effects in the pandemic outbreak. Coven, Gupta, and Yao (2022) confirm that the disease spreads along urban flight networks, while the first part of our analysis establishes the spread of COVID-19 across London boroughs through commuting networks. Chandrasekhar, Goldsmith-Pinkham, Jackson, and Thau (2021) also demonstrate that network key players are crucial targets for partial lockdowns through simulation studies of a theoretical network model. The second part of our study comprehensively evaluates optimal lockdown plans using real parameter estimates for the spread of COVID-19 in London.

1 A Network SIR Model

This section introduces our network SIR model. We first extend the deterministic single-population SIR model to its stochastic counterpart and derive necessary distributional results for mapping the model to disease surveillance data. Then, we extend the statistical model to multiple subpopulations, with a special account for network effects, formalising a network SIR framework. Finally, we enrich the framework by introducing a parametrisation scheme tailored for analysing the spreading of COVID-19 in London.

1.1 The deterministic SIR dynamics

We begin with notation. For a given population of fixed size N , the triplet $\{S_t, I_t, R_t\}$ represents, respectively, the *cumulative* numbers of susceptible (S), infectious (I), and recovered (R) individuals at time t . Susceptible individuals get infected through mixing with infectious individuals, featuring the dynamic

$$\dot{S}_t = -\theta_I \frac{I_t}{N} S_t, \quad (1)$$

in which the overdot notation represents derivatives with regard to time; I_t/N is the level of disease prevalence in the current population (N); θ_I is a parameter measuring the contact rate (times the probability of infection per contact). Infected individuals recover at a rate θ_R , which implies

$$\dot{R}_t = \theta_R I_t. \quad (2)$$

The sum $S_t + I_t + R_t$ equals the total population N , constant by assumption. Therefore, $\dot{S}_t + \dot{I}_t + \dot{R}_t = 0$. Plugging in (1) and (2) and rearranging terms,

$$\dot{I}_t = \left(\theta_I \frac{S_t}{N} - \theta_R \right) I_t. \quad (3)$$

Our analysis will focus on the dynamics of the infected population I_t . For expositional purposes, in the main part of the paper we make the simplifying assumption that $S_t/N \approx 1$,

but we also derive and estimate a more general model that does not impose this restriction. For COVID-19 in London, the S_t/N ratio is greater than 99.7% in our sample period. Treating each London borough separately, this ratio ranges from 99.6% (Brent, four cases per thousand population) to 99.8% (Islington, two cases per thousand population). Based on this assumption, a constant, namely α , defined as $\alpha \triangleq \theta_I - \theta_R \approx \theta_I S_t/N - \theta_R$, is sufficient to capture the dynamics of the infectious and infected subpopulations in our sample.

Assuming $S_t/N \approx 1$, we can reduce the SIR model to a stochastic process for the number of infections. Dropping this simplification, our framework can be generalised to allow, as we do in Appendix C, time variation in α due to the changing fractions of susceptible individuals.²

1.2 The stochastic SIR model

To map the deterministic SIR model to the data, we need to introduce probabilistic “error” terms. However, arbitrarily introduced errors such as Gaussian errors may reduce statistical power due to misspecified likelihood functions. The issue is more pronounced when the number of disease incidents is relatively small (compared with the total population size), which is the case in our data (less than three detected cases per thousand people in London by the end of the lockdown period). Thus, we aim to derive this distribution coherently from a well-defined probabilistic analogue to the deterministic SIR dynamics. The natural stochastic extension to the differential equation $dI_t/dt \approx \alpha I_t$ is a continuous-time Markov chain of the form:

$$\mathbb{P}[y \text{ new infections in } (t, t + dt) \mid I_t = x] = \begin{cases} \alpha x dt, & y = 1 \\ o(dt), & y \geq 2, \\ 1 - \alpha x dt - o(dt), & y = 0 \end{cases}, \quad (4)$$

where $o(dt)$ satisfies $o(dt)/dt \rightarrow 0$ as $dt \rightarrow 0$. Interpreting this probabilistic statement is straightforward. Given the current number of infective individuals x , within an infinitesimally short time interval, one additional person can contract the disease with probability $\alpha x dt$. This random process is a simple birth process (also known as the Yule-Furry process, see for example, [Grimmett and Stirzaker \(2001, p. 250\)](#)).

When working with surveillance data of infectious diseases, we only observe numbers of new cases within discrete time intervals (say, one day or one week). Based on the specification (4), we can solve for the distribution of new case counts within a time interval of length h (instead of length dt which goes to zero), denoted by

$$p_h(y \mid x) = \mathbb{P}[y \text{ new infections in } (t, t + h) \mid I_t = x].$$

²Allowing α to vary over time our findings are *quantitatively* the same, reconfirming the empirical validity of assuming $S_t/N \approx 1$ for every London borough during the first wave of COVID-19 pandemic from March to June 2020.

Solving the implied Kolmogorov forward equation (see [Grimmett and Stirzaker \(2001, p. 250\)](#)), the simple birth process in (4) yields an analytical expression of the probability mass function $p_h(y | x)$:

$$p_h(y | x) = \frac{\Gamma(y+x)}{\Gamma(x)\Gamma(y+1)} \left(e^{-\alpha h}\right)^x \left(1 - e^{-\alpha h}\right)^y, \quad (5)$$

where $\Gamma(\cdot)$ represents the gamma function. The above expression describes a negative Binomial distribution – a mixture of Poisson distributions with mixing of the Poisson rate driven by a gamma distribution. It provides the chance of y successes after exactly x failures in a sequence of independent Bernoulli trials, each having a probability of success $p = 1 - e^{-\alpha h}$. The negative Binomial is an appropriate representation for discrete arrival data over an unbounded positive range whose sample variance exceeds the sample mean. In such cases, the observations are overdispersed with respect to a Poisson distribution (for which the mean is equal to the variance). Since the negative binomial distribution has one more parameter than the Poisson distribution, the second parameter can be used to adjust the variance separately from the mean. Furthermore, it implies that first and second conditional moments are positively correlated – a feature consistent with epidemic dynamics. The probability $p (= 1 - e^{-\alpha h})$ also has a clear interpretation in our context of disease transmission. Let $y = 0$ and $x = 1$ in (5), then p is the probability that an existing disease case infects *at least* one person within a period of length h (since $e^{-\alpha h} = 1 - p = p_h(0 | 1)$, implying that $p = 1 - p_h(0 | 1) = \sum_{y \geq 1} p_h(y | 1)$).

Denote the daily count of new infected individuals as y_t , $t = 1, \dots, T$. Normalising the length of the time interval h to one day and denoting with \mathcal{F}_t the information available up to time t , we have

$$y_t | \mathcal{F}_{t-1} \sim \text{NegBinom}(p, x_{t-1}), \quad (6)$$

where $p = 1 - e^{-\alpha}$. Conditional expectations of new disease cases can be computed directly as

$$\mathbb{E}[y_t | \mathcal{F}_{t-1}] = \mu_t = ax_{t-1} \quad (7)$$

where $a = e^\alpha - 1 = p/(1 - p)$ can be understood as the odds ratio comparing the probability that an infected person does transmit the disease against that he does not. This simple linear relationship between the conditional expectations of new case numbers and existing infectious individuals is the key modelling assumption that we adopt throughout our analysis. Equation (1.2) also implies that

$$p = \frac{\mu_t}{x_{t-1} + \mu_t} \quad (8)$$

which offers a simple mapping from the conditional expectations μ_t to the probability parameter p in the negative binomial distribution (5).

From the negative binomial distribution, we can also calculate the conditional variance of

new case counts as

$$\text{var}[y_t \mid \mathcal{F}_{t-1}] = (a+1)ax_{t-1}. \quad (9)$$

If $a+1 = 1/(1-p) \rightarrow 1$, that is $p \rightarrow 0$, which means that the disease transmission rate is extremely small, the conditional variance of y_t equals its conditional mean. This corresponds to a Poisson distribution specification for y_t as $y_t \sim \text{Pois}(ax_{t-1})$. Equations (1.2) and (9) imply a positive correlation between the first and second moments for the number of new infected individuals – a feature consistent with the data under analysis.

The remaining issue is how to determine the number of *actively* infectious cases x_t . This issue arises because people who have been infected might recover (or they may die), as we have initially discussed in the SIR model. We adopt the following formulation for x_t :

$$x_t = \sum_{\ell=0}^{L-1} \nu(\ell) y_{t-\ell}, \quad (10)$$

which assumes that infected individuals can transmit the disease for L periods. The decay function $\nu(\ell) \in (0, 1)$ characterises “the rate of infectivity,” in the language of [Kermack and McKendrick \(1927\)](#).³ That is, for a person who has been infected for ℓ periods, the chance of transmitting the disease to another person is reduced to $100 \times \nu(\ell)$ percent of the initial level. Another way of interpreting this specification is that $100[1 - \nu(\ell)]$ percent of the infected individuals are no longer infectious ℓ periods after having contracted the disease.

1.3 A stochastic network SIR model

Now, we extend the stochastic model introduced above to account for multiple subpopulations connected in a network. In the context of the COVID-19 spread in London, we treat London boroughs as subpopulations of constant sizes N_i , $i = 1, \dots, n$. Time- t conditional expectations of new case counts are concatenated into a vector $\mu_t = [\mu_{1t}, \dots, \mu_{nt}]^\top$, where $\mu_{it} = \mathbb{E}[y_{it} \mid \mathcal{F}_{t-1}]$ is the expected number of new cases in borough i at time t . The distribution of newly infected individuals y_{it} follows the negative Binomial structure in (6)–(8), specified as follows:

$$y_{it} \sim \text{NegBinom}(p_{it}, x_{i,t-1}) \quad \text{where} \quad p_{it} = \frac{\mu_{it}}{x_{i,t-1} + \mu_{it}}. \quad (11)$$

To extend the conditional mean equation (1.2) to the multivariate case, we specify μ_t as

$$\mu_t = Ax_{t-1} + \mu_t^{EN} = \underbrace{\mu_t^{AR}}_{\text{diag}(A)x_{t-1}} + \underbrace{\mu_t^{NE}}_{(A - \text{diag}(A))x_{t-1}} + \mu_t^{EN} \quad (12)$$

³The simple SIR, especially that with constant rate of recovery as in (2), is a tractable special case considered in [Kermack and McKendrick \(1927\)](#). In the general setup of their model, constant rate of recovered is replaced with a specification similar as in (10).

where $\mathbf{x}_t = [x_{1t}, \dots, x_{nt}]^\top = \sum_{\ell=0}^{L-1} \nu(\ell) \mathbf{y}_{t-\ell}$ is the vector of infectious individuals in the London boroughs and A is an $n \times n$ matrix of coefficients. The first term in (12), $A\mathbf{x}_{t-1}$, and the definition of \mathbf{x} , imply *vector* autoregressive dynamics in the disease propagation. The additional term μ_t^{EN} , which we call the *endemic* term, aims to capture variations in disease dynamics that are not explained by the *epidemic* component $A\mathbf{x}_{t-1}$. Such endemic forces aim to accommodate seasonality, behavioural responses, or transmission dynamics induced by external forces.⁴ This endemic/epidemic decomposition is commonly adopted in the empirical analysis of epidemiological surveillance data (see, e.g. [Finkenstädt and Grenfell \(2000\)](#), [Held, Höhle, and Hofmann \(2005\)](#), [Lawson \(2013\)](#)).

By further separating the endemic effect in equation (12) into its intra- and inter-borough elements, we have a natural decomposition of the conditional expectation of new infections into three components: the local (intra-borough) autoregressive effects μ_t^{AR} , the network (inter-boroughs) effects μ_t^{NE} , and the endemic effects μ_t^{EN} .

Autoregressive effects. The local autoregressive effects capture disease dynamics as if each subpopulation were in isolation – i.e., as if new cases were driven only by infectious residents within the same borough. These are equivalent to assigning the single-population dynamic in equation (1.2) independently for each subpopulation. We adopt the simplest specification for the autoregressive effects by treating them as homogeneous among subpopulations. This implies that $\text{diag}(A) = \gamma I$, where the coefficient γ can be understood as the odds ratio parameter a in equation (1.2).⁵

Network effects. Moving from one homogeneous population to multiple subpopulations, a key new component is the network effects μ_t^{NE} , which is the main focus of our analysis. These effects are driven by a network (or multiple networks) of connections between subpopulations. Individuals contact and transmit the disease along predefined network links; the intensity of transmission is captured by the “strength” of links (i.e., varying edge values of the network). These network effects of disease transmission have long been acknowledged and were brought to light by [Newman \(2002\)](#). The network effects can also be interpreted as matching intensities between individuals from different subpopulations as in [Acemoglu, Chernozhukov, Werning, and Whinston \(2021\)](#). In particular, given an observable adjacency matrix $W = \{w_{ij}\}_{1 \leq i,j \leq n}$ capturing the connections among London boroughs, we model the network effects μ_t^{NE} in (12) as

$$\mu_{it}^{NE} = \phi \left(\sum_{j \neq i} w_{ij} x_{j,t-1} \right). \quad (13)$$

Under this formulation, for residents of borough i , the chance of being infected by residents

⁴This is to be partially distinguished from the concept of “endemic diseases”, which command stationary transmission dynamics due to the combination of slow propagation rate and temporary immunity.

⁵The specification is easily generalisable to location specific local dynamics by setting $\text{diag}(A) = \text{diag}(\{\gamma_j\}_{j=1}^n)$.

from borough j is proportional to the strength of connections between the two boroughs, as described by the network topology W . The constant ϕ determines the overall strength of these network effects. The specification in (13) can be extended to allow for multiple networks, with adjacency matrices given by $W^{(g)} = \{w_{ij}^{(g)}\}_{1 \leq i,j \leq n}$, $g = 1, \dots, G$, as follows:

$$\mu_{i,t}^{NE} = \sum_{g=1}^G \phi^{(g)} \left(\sum_{j \neq i} w_{ij}^{(g)} x_{j,t-1} \right). \quad (14)$$

Here, the topology specific coefficients $\phi^{(g)}$ capture the strength of the disease propagation through the various sets of links considered.

The above assumptions about the autoregressive and network effects directly translate into a parametric specification for matrix A in (12):

$$A = \gamma I + \sum_{g=1}^G \phi^{(g)} W^{(g)}. \quad (15)$$

Hence, our formulation implies that the conditional expectation of new infections is driven by both local autoregressive, as well as spatial, dynamics.

The set of parameters $\{\gamma, \phi^{(1)}, \dots, \phi^{(G)}\}$, jointly with the adjacency matrices $W^{(g)}$, fully determine matrix A , which is essential for understanding the disease transmission dynamics. We expect these parameters to be non-negative for the data-generating process to be well defined, and impose this restriction by working with exponential forms. Furthermore, as the lockdown policy may affect these fundamental parameters, we model them as time varying. That is:

$$\gamma \equiv \gamma_t = \exp(\gamma_0 + D_t \gamma), \quad (16)$$

$$\phi^{(g)} \equiv \phi_t^{(g)} = \exp(\phi_0^{(g)} + D_t \phi^{(g)}), \quad g = 1, \dots, G, \quad (17)$$

where $D_t \in \{0, 1\}$ is a dummy variable equal to zero before the lockdown and one afterwards. The impact of the policy change is therefore quantified as $\exp(\gamma)$ for autoregressive effects and $\exp(\phi^{(g)})$ for network effects, multiplicatively. For example, if $\exp(\gamma) = 0.70$, then the policy reduces the local autoregressive effects by $100 \times (1 - 0.7)\% = 30\%$.

Endemic effects. The endemic effects in (12) are specified as

$$\mu_{i,t}^{EN} = \exp(z_t^\top \beta + \eta_i) N_i, \quad i = 1, \dots, n \quad (18)$$

which is proportional to the size of subpopulations N_i . The vector z_t contains deterministic time trends such as polynomial and trigonometrical functions of time t . Additional time-varying terms for control, such as time fixed effects and time-varying testing intensity and positive-to-test ratio, are also included in this vector when introduced in our robustness analysis.

ysis. Location-specific fixed effects η_i , are added in the endemic terms to account for static demographic and socioeconomic heterogeneities among subpopulations. In particular, control variables in the endemic term are specified as $z_t = [t, t^2, t \times D_t, t^2 \times D_t]$.

Linear and quadratic terms of time are motivated by the hump-shaped disease spread trend (see, e.g., [Li and Linton \(2021\)](#)). These deterministic trends are allowed to change after the lockdown policy, with two interaction terms, $t \times D_t$ and $t^2 \times D_t$, added in, to reflect changing endemic forces after the lockdown.⁶

Estimation of the model parameters is performed via maximum likelihood. The tuning parameter ρ of the exponential decaying kernel $v(\ell) = \exp(-\rho\ell)$ is selected via (maximising) the profile likelihood of each model, and we also conduct a sensitivity analysis with respect to this key persistency parameter. Standard errors are all calculated based on the outer product of the score vectors à la [Berndt, Hall, Hall, and Hausman \(1974\)](#).

We focus on performing inferences about parameters that determine the epidemic (autoregressive and network) effects. For parameters governing the baseline (before-policy) disease spread dynamics, we test whether their exponentials are significantly greater than zero, that is, $\exp(\gamma_0) > 0$ and $\exp(\phi_0^{(g)}) > 0$ for all $g \in \mathcal{G}$ are our null hypotheses. These tests evaluate if there are substantial autoregressive or network effects during the COVID-19 pandemic in London. For parameters quantifying the policy impacts, we ask if their exponentials are significantly smaller than one, that is, if our null hypotheses are $\exp(\gamma) < 1$ and $\exp(\phi^{(g)}) < 1$. This is because (the exponentials of) these parameters all measure (gross) percentage changes from baseline estimates after the lockdown policy is implemented.

2 Data and Estimation

This section surveys the multiple data sources, including networks of London boroughs we use in this study, and presents estimation results and their implications.

2.1 COVID-19 data and demographic information

Disease surveillance data are provided by the UK government.⁷ This database reports the number of daily new cases found in each local authority of the UK. We focus on local authorities of London, consisting of 32 London boroughs.⁸ Our sample period is from March 1 to June 4, 2020. We begin our analysis from March because the number of reported cases is

⁶For robustness, we also consider two additional variables, the (seven-day moving averages of) positive-to-test ratio and the number of tests across all London boroughs to account for common variation across time due to limited testing capacity, especially in the early stage of the disease outbreak in UK.

⁷<https://coronavirus.data.gov.uk/>

⁸The city of London, strictly speaking, is not an official London borough (but, still a local authority), and in our dataset it is merged with Westminster. It is noteworthy that the city of London has an extremely small number of residents (less than ten thousand) and only thirteen disease cases in total (till June 4, 2020).

small from January to February in London.⁹

We illustrate in Panel (A) of Figure 1 the total number of reported COVID-19 cases in each borough until June 4, 2020. In general, the number of cases of the pandemic in each borough correlates with subpopulation sizes, which is shown in Panel (B) of the same figure. The correlation is 0.78 throughout our sample period. This association corroborates our specification for the endemic terms in equation (18), which is proportional to the subpopulation sizes.

There are three major policy dates for COVID-19 in the UK. They are March 16 when citizens were recommended to avoid traveling and stay home, March 20 when schools and pubs were closed, and March 23 from which full nationwide lockdown measures became effective. We choose March 23 as our baseline policy date and evaluate the impacts of nationwide lockdown measures on the autoregressive and network effects using the specifications in (16) and (17). Furthermore, in our robustness analysis, we allow all of the parameters to change at the above mentioned policy dates.

Additionally, for subpopulation (borough) sizes, we use records from a housing-led population projection conducted by the Greater London Authority (GLA).¹⁰ The GLA demography team constructs these projections based on trends in fertility, mortality and migration, and housing development on an annual basis. The starting point of these projections is dwelling records from the 2011 UK census.¹¹

We use the UK nationwide testing data from the GitHub repository of Our World in Data (OWID).¹² Since May 23, 2020, the UK government has stopped publishing data regarding the number of “people tested”. OWID uses instead the official data for the number of “tests performed” since then. For these numbers, only official swab tests count and all serology tests are disregarded.¹³

To measure the reduction in workplace activities for each London borough after the March 23 lockdown and inform our counterfactual calibrations, we use Google’s COVID-19 Community Mobility Reports, which is publicly available for the pandemic periods.¹⁴. The Google mobility measures are constructed from cell phone tracking data and also used by Farboodi et al. (2021) and Chernozhukov et al. (2021) to calibrate reductions in social activities due to policy restrictions.

⁹There are only fifteen cases in total, with Southwark borough having the largest number, which is only three.

¹⁰Link: <https://data.london.gov.uk/dataset/housing-led-population-projections>

¹¹Population census across all four UK countries is taken every ten years. The 2011 census is the most recent. We also use the census data for constructing our networks, as we discuss below.

¹²Link: <https://github.com/owid/covid-19-data/tree/master/public>

¹³Official swab tests are those conducted in Public Health England (PHE) labs and National Health Service (NHS) hospitals, as well as those processed *in-person* under government guidance for a wider population. Swab tests for surveillance purpose undertaken by PHE, Office for National Statistics (ONS), Biobank, universities, and other partners do not count.

¹⁴See <https://www.google.com/covid19/mobility>

2.2 Network construction

We construct networks connecting residents of different boroughs through commuting links. We use data from the 2011 UK Census to create a *directed* and *weighted* graph, of which 32 nodes denote the London boroughs¹⁵. Edges of this graph quantify employment links between boroughs. For example, an edge of value 10,000 from Camden to Southwark means that there are 10,000 individuals living in Camden who go to work in Southwark. We ignore all self-pointing edges, meaning that we drop the numbers of people working in the same boroughs where they live, since the local effects are already meant to be captured by the autoregressive component μ_t^{AR} . In other words, the adjacency matrix of this graph has a diagonal of constant zeros.

This graph is visualised in Figure 2. The size of a node in this figure is proportional to its in-degree (total number of people coming to work in this borough). For clarity, an edge is drawn only if its value exceeds the 80% percentile of all edge values. Widths of these plotted edges are also proportional to their values. A clear pattern of Figure 2 is that Westminster/City of London attracts a disproportional amount of London workforce with a total in-degree that is significantly larger than any other London borough. In addition, Camden and Tower Hamlets also attract a relatively large amount of workforce.

We denote by $K = \{k_{ij}\}_{1 \leq i, j \leq n}$ the adjacency matrix of this graph, where i indexes home and j indexes work. We have constructed other networks based on this K matrix. Specifically, we consider three networks, $W^{(1)} = K$, $W^{(2)} = K^\top$, and $W^{(3)} = KK^\top$, defined respectively through adjacency matrices.¹⁶ These three adjacency matrices capture transmission from different contact networks: 1) “work-to-home” transmission, which measures the spreading of disease from residents in commuter’s work borough to residents in commuter’s home borough; 2) “home-to-work” transmission, which is from the opposite direction; and 3) “home-to-home” transmission, which is between different places of residence via a common workplace.

Generally speaking, left-multiplying the vector of active cases x_t by the matrix $W^{(1)}$ as in equation (14) features the transmission of COVID-19 from workplaces to residential areas. To be clear, for borough i , the vector $[w_{ij}^{(1)}]_{j \neq i}$ will *overweight* boroughs where more of borough i ’s residents go to work. For example, for many London boroughs, their residents are more likely

¹⁵The 2011 census covers detailed employment information which includes office locations. Thus, for any local authority, the number of its people working in other local authorities can be calculated. Aggregate data regarding these statistics are available from <https://data.london.gov.uk/dataset/place-residence-place-work-local-authority>.

¹⁶Notations here are to provide basic ideas. In detail, when estimating the network SIR models, we always divide K and K^\top by the largest singular value of K to rescale their spectral norms to one. This operation improves numerical stability (of nonlinear maximum likelihood estimation) and ensures comparability across network parameters. For computing the adjacency matrix of the third network, namely $W^{(3)}$, we first normalise each row of K to sum one, then calculate the product of it with its transpose. Diagonal elements of this product are also replaced with zero. The resulting matrix is then divided by its largest singular value (which is also its largest eigenvalue because this matrix is symmetric).

to go to work at Westminster/City of London. Thus, the propensity for contact and infection *from* Westminster/City of London is set to be higher by this network. Intuitively, larger nodes of the graph shown in Figure 2 are more emphasised in the transmission dynamics.

Similarly, left multiplying x_t by $W^{(2)}$ characterises the disease spread from residential areas to workplaces. Panel (A) of Figure 3 shows the graph defined by $W^{(2)}$. Edges are again thresholded at the 80% for presentation. Node sizes are also proportional to their total in-degrees. As we can see from Panel (A) of Figure 3, network effects commanded by this graph highlight the role of boroughs such as Wandsworth, Lambeth, Lewisham, and Southwark. These boroughs are those with large numbers of residents going to work in other boroughs.

Interpreting the impact of our third network on the disease spread dynamics – the home-to-home network – is also straightforward. The adjacency matrix of this network is symmetric with element (i, j) and (j, i) defined by $\sum_{\ell=1}^n k_{i\ell} k_{\ell j}$. It quantifies the propensity of residents of borough i and j to contact and infect each other with the disease via common workplaces. Specifically, if work and home locations were independent, the entries of this particular adjacency matrix would be proportional to the probability of individuals from the two locations meeting each other. Panel (B) of Figure (3) visualises the graph of this network. Nodes with large in-degrees such as Westminster/City of London, Camden, and Tower Hamlets should be influential in driving the disease spread dynamics mediated through this network. These boroughs are also featured in the work-to-home network graphed in Figure 2. In addition, Wandsworth, Lambeth, and Southwark, which emerge as pivotal nodes in the home-to-work graph, are also highlighted here, meaning that boroughs with large numbers of residents working outside those boroughs also have strong network effects. An exception to this appears to be Lewisham, which does not appear to be influential in the graph.

One limitation of the three transmission networks we have considered so far is that they all ignore the possibility of transmission simply due to “co-traveling”. That is, instead of getting infected due to contacts at workplaces or residences, people can get the virus while traveling within the Transportation for London (TfL) network. To quantify the network effects of traveling together at the borough level, we need to measure how likely residents from two different boroughs can meet in the TfL network while they do not necessarily head towards the same destination.

We present a simple approach to quantify this “co-traveling” network in Appendix D, assuming people travel along the shortest paths along the TfL network. The resulting network looks differently from our “work-to-home”, “home-to-work”, and “home-to-home” transmission networks. The boroughs highlighted in this network include (see Figure A1 in Appendix D) Wandsworth, Haringey, Waltham Forest, and Hackney, which belong to the outer zones of London. Residents of these boroughs are more likely to travel through busy TfL nodes and links. Thus their paths are more likely to cross with residents from other boroughs.

3 Empirical Findings

The main estimation results are presented in Table 1. Five specifications are included: three specifications with one of the networks ($\mathcal{G} = (1), (2), (3)$) each; one specification containing all three networks ($\mathcal{G} = (1, 2, 3)$); and one specification incorporating the first two networks ($\mathcal{G} = (1, 2)$). The first three specifications serve the purpose of univariate analysis. Parameter estimates and standard errors are reported in the table, as well as the pseudo- R^2 defined as

$$\text{pseudo-}R^2 = 1 - \frac{\sum_{i=1}^n \sum_{t=1}^T (y_{it} - \hat{\mu}_{it})^2}{\sum_{i=1}^n \sum_{t=1}^T (y_{it} - \bar{y})^2},$$

where $\hat{\mu}_{it}$ is the conditional expectation of daily new COVID-19 cases calculated from the model using estimated parameters; \bar{y} stands for simple average across time and boroughs.

Before-policy estimations for the autoregressive effects, that is, estimates of $\exp(\gamma_0)$, are always significantly greater than zero. Across the five specifications, the smallest estimate is 0.340 with a standard error of 0.037. As this parameter quantifies within-borough disease transmission dynamics, this finding confirms that serious community-acquired infection has occurred during the initial outbreak of COVID-19 in London in early 2020. The nationwide lockdown policy on March 23 has reduced the infection significantly: the magnitude of reduction is at least 47%. The reduction is statistically significant as $\exp(\gamma)$ is always significantly smaller than one. The analysis shows that the lockdown policy is effective in cutting down within-community transmission rates.

Estimation results from the first specification (column 1 of Table 1) show that the impact of the work-to-home network is large in magnitude: the before-policy coefficient $\exp(\phi_0^{(1)})$ is around 0.56, which implies strong directional spillover effects from people living in major workplaces such as Westminster/City of London to residents in other boroughs via the work-to-home contact network. We also find that the work-to-home disease spread is partially reduced after the lockdown. The magnitude of reduction is around 20% for the first specification, while being not statistically different from one at 1%. The effectiveness of the lockdown policy on blocking cross-borough transmission seems questionable. After controlling for the other two networks, the reduction is around 35%, and is statistically significant. Given these findings, we do not have a conclusive evidence that the nationwide lockdown stopped the transmission from pivotal places such as Westminster/City of London, Camden, and Tower Hamlets to other boroughs.

We find that the impact of the home-to-work network on the epidemics of COVID-19 in London is relatively small (column 2 of Table 1). The baseline estimation $\exp(\phi_0^{(2)})$ is around than 0.07.¹⁷ This parameter is around 0.04 after controlling for other contact networks.

¹⁷Our parameter estimates for different networks are comparable because all graph adjacency matrices have been rescaled by their largest singular value before feeding into our models.

Though smaller in magnitude, it is significantly greater than zero at the 1% level except for the last specification. We find that the lockdown policy has a stronger impact on this home-to-work spreading. After the lockdown policy is enforced, the spreading through home-to-work network is reduced by over 80% after controlling for the work-to-home transmission network.

We find a strong home-to-home network effect when estimating it alone (column 3 of Table 1), but it is insignificant after controlling for the previous two networks (column 4 of Table 1). Thus, we choose to use the last specification including both work-to-home and home-to-work networks as the benchmark specification (column 5 of Table 1). The maximised log-likelihood function for the fourth and the fifth specifications are -7317.64 and -7315.88 , respectively. A likelihood ratio test simply fails to offer any definitive evidence on including the home-to-home network. Therefore, we report further analyses of the network effects based on this benchmark specification for expositional clarity in the rest of the paper.

To determine if our findings are sensitive to the functional forms included into the vector z_t (determining the endemic effects), we report in Table 2 the parameter estimates after replacing $z_t^\top \beta$ by ξ_t , with all $\{\xi_t\}_{t=1}^T$ treated as model parameters. This is effectively controlling for time fixed effects at the daily frequency. We can confirm our findings regarding transmissions with boroughs (autoregressive effects) as well as transmissions along the work-to-home (stronger) and home-to-work networks (weaker). The only difference from our baseline estimation is that the March 23 nationwide lockdown now seems to have more conclusive effects on *both* the work-to-home and home-to-work transmission channels. In Appendix Table A5, we repeat the analysis by controlling for time fixed effects at the weekly frequency, which yields similar findings to our baseline estimations.

Adjusting for testing capacities in the early stage of COVID-19 transmission, we report in Appendix Table A4 estimation results that include the positive-to-test ratios and lagged testing numbers into the vector z_t . Our main parameter estimates remain similar.

Simpler networks as baseline settings. To confirm that the commuting networks we consider do convey useful information to explain the cross-borough transmission dynamics, we consider three simple alternative specifications of the matrix A in equation (12) as baseline cases. These specifications include (i) a diagonal matrix which is determined by the population size of each borough, i.e., $A = \gamma I + \phi \text{diag}\{N_1/N, \dots, N_n/N\}$; (ii) a compound symmetric specification for the network effects, i.e., $A = \gamma I + \phi W^{(\text{cs})}$ in which all off-diagonal elements of $W^{(\text{comp})}$ are the same and equal to the average of elements in K (the work-to-home network); (iii) a square exponential kernel specification for the network effects, i.e., $A = \gamma I + \phi W^{(\text{se})}$ in which $W_{ij}^{(\text{se})} = \exp(-100d_{ij}^2)/10$ with d_{ij} being the distance between the centroids of borough i and j . Of note, the choice of kernel parameters is made such that the elements in $W^{(\text{se})}$ are of a similar magnitude to K .

Table 3 reports the estimation of our model after replacing the three commuting networks

with the simple network structures discussed above. The estimates of the autoregressive effects (within-borough transmission) are similar to the ones reported in Table 1. Among these different versions of A , only the compound symmetric and square exponential kernel specifications appear useful to capture the network effects. After including all three networks, only the compound symmetric network demonstrates statistically significant contributions to the cross-borough COVID transmission. This finding suggests that the transmission between different boroughs do contribute to the pandemic outbreak: even this simplest network structure can capture some of effect.

We also report the difference between the Akaike information criteria (AIC) of these three simple networks and our preferred model $\mathcal{G} = (1, 2)$ (i.e., including both the work-to-home and home-to-work networks) in Table 3. Model fittings under these three alternative networks, individually or jointly, are worse as their AIC metrics are consistently larger. To further “horse-race” these three alternative networks against our preferred model $\mathcal{G} = (1, 2)$, we present in Table 4 the estimation results of adding the diagonal, compound symmetric, and (square exponential) kernel-based networks to the work-to-home and home-to-work networks. With the two commuting networks included, none of the alternative networks demonstrate significant impacts on the cross-borough transmissions. Adding any one of the alternative networks to our preferred model leads to higher AIC and thus becomes less favoured by data.

The network of “co-traveling”. As we have pointed out in Section 2.2, our analysis so far ignores the possibility of COVID transmissions due to contagions while traveling in the TfL networks. We present an approach to construct a network characterising this transmission mechanism due to “co-traveling” in Section D of the Appendix. Table A2 tabulates the effects of contracting the virus while traveling together in the London underground. Including the co-traveling network in our analysis largely does not affect our parameter estimates reported in Table 1.

The autocorrelation structure. Our results are robust to alternatively specified temporal dependence structure, which is determined by the parameter ρ . Recall that the number of actively infectious cases is $x_t = \sum_{\ell=0}^L \exp(-\rho\ell)y_{t-\ell}$. As a result, the parameter ρ effectively defines an autocorrelation structure for the stacked vector $[y_t^\top, y_{t-1}^\top, \dots, y_{t-L+1}^\top]^\top$ (see Appendix B for detailed exposition). We choose $\rho = 0.8$ via profile likelihood for our main results reported in Table 1 (Figure 4 plots the profile likelihood function). We perturb ρ around its optimal value 0.8 and refit the preferred model specification $\mathcal{G} = (1, 2)$. Table A3 reports the parameter estimates for this model with $\rho \in \{0.4, 0.6, 0.8, 1, 1.2\}$. We can always confirm the importance of network effects under different autocorrelation structures; estimates for the March 23 lockdown policy’s impacts on network effects are extremely stable. Changing autocorrelation structure mainly affects our estimates for the within-borough transmission dynamics. As expected, smaller values for ρ , equivalent to larger numbers of accumulated infectious cases x_t , lead to smaller parameter estimates for γ . However, as $\rho \geq 0.6$, parameter

estimates for the within-borough effects also become stable.

Joint analysis of multiple policy dates. As we have mentioned before, in addition to the March 23 (namely t_3) nationwide lockdown, there are two other policy dates worthwhile examining: March 16 (namely t_1) when stay-at-home recommendations were made and March 20 (namely t_2) when schools and pubs were closed. Our framework is flexible enough to incorporate these additional policy dates by letting $D_t = \{I_{\{t_1 < t \leq t_2\}}, I_{\{t_2 < t \leq t_3\}}, I_{\{t > t_3\}}\}$. Table A6 of the Appendix reports the results. Our parameter estimates for COVID-19 spreads in London before any public policy interventions are similar to ones reported in Table 1 (before March 23). For the first two policy dates, we generally cannot find any meaningful policy impacts on the first network (i.e., $\phi^{(1)}$ are close to zero or equivalently $\exp(\phi^{(1)}) = 1$). These two earlier policies seem to reduce transmissions along the second network. However, we do not have enough power to conclude that they are statistically significant (i.e., we cannot reject $\exp(\phi^{(2)}) \neq 1$), mainly due to the small time windows.

3.1 Decomposition of expected daily new cases

We now plug the estimated parameters into expected new case numbers μ_t as defined in (12) to evaluate and compare the contribution of autoregressive, network, and endemic components in explaining the observed data. We rely on parameter estimates from the benchmark specification incorporating the work-to-home and home-to-work networks (column 5 in Table 1) to perform this decomposition in this section.

Panel (A) of Figure 5 graphs the decomposition of the contribution of the autoregressive, the network, and the endemic components to the total cases aggregating across the 32 London boroughs in the sample period. That is, we plot the time-series of the three ratios $(\mathbf{1}^\top \hat{\mu}_t^{AR}) / (\mathbf{1}^\top \hat{\mu}_t)$, $(\mathbf{1}^\top \hat{\mu}_t^{NE}) / (\mathbf{1}^\top \hat{\mu}_t)$, and $(\mathbf{1}^\top \hat{\mu}_t^{EN}) / (\mathbf{1}^\top \hat{\mu}_t)$ as defined in Section 1.3. The graph demonstrates a substantial and persistent network effect, accounting for 60% of the expected total daily new cases in London before the March 23 lockdown (38% after). The autoregressive and endemic effects contribute to 40% and 34% before and after the lockdown date. Our estimation result also suggests that endemic terms are not needed to explain daily new COVID cases before the lockdown. After the lockdown, around 28% of expected new cases each day can be attributed to endemics.

In Panels (B) and (C) of the same figure, we present the decomposition result for each London borough. We plot the time series of the fractions of conditional means explained by each of the three components, $\hat{\mu}_{it}^{AR} / \hat{\mu}_{it}$, $\hat{\mu}_{it}^{NE} / \hat{\mu}_{it}$, $\hat{\mu}_{it}^{EN} / \hat{\mu}_{it}$, for each borough. Light-coloured bands in these plots show 10% to 90% percentiles across all boroughs, delineating cross-sectional heterogeneity. Solid lines represent the median levels.

The left graph in Panel (B) shows community transmission (autoregressive effects) rises quickly and remains a strong driver of the disease spread since March. The middle graph in

Panel (B) shows peaked network effects contributing to the spread of COVID in London in early March 2020. As cases accumulate, community transmission starts to catch up, partly crowding out the dominant role of transmission along the commuting networks across boroughs.

In Panel (C) of Figure 5 we further decompose the network effects by examining the contributions of the work-to-home and the home-to-work network to the total network effect across time in our sample period, respectively. Based on plots in this panel, we observe that almost all network effects in our sample period can be attributed to the work-to-home network, highlighting the importance of boroughs where many people go to work in transmitting the disease. This finding results from parameter estimates in Table 1, where the network coefficient for the second specification $\exp(\phi_0^{(2)})$ is more than ten times smaller than its counterpart for the first specification $\exp(\phi_0^{(1)})$. Although weaker in terms of magnitude, we also observe that the home-to-work network effects have undergone much stronger reduction after the lockdown policy (i.e. $\exp(\phi^{(2)}) < \exp(\phi^{(1)})$).

Panel (C) further shows that the reductions in the fraction of expected new cases due to the work-to-home network effect have occurred at least two weeks before March 23. This is due to the increased contributions to the infection propagation coming from the autoregressive component. This mechanism is also quite intuitive: community transmission within boroughs becomes pronounced *after* the number of infected individuals accumulates through the network transmission.

3.2 Disease R_0

Our model offers guidance on the basic reproduction number R_0 , which quantifies the expected number of new cases *directly* generated by one existing case. To be more specific, since our model features borough-level heterogeneity, the expected number of new cases varies with regard to the residence of the existing infected cases. Thus, if the “one” existing case comes from borough i , we have a basic reproduction number $R_0^{(i)}$. What we aim to compute here is an estimated upper bound on the maximum $\max_{i \in \{1, \dots, n\}} R_0^{(i)}$.

To proceed, we first calculate a simple plugging-in estimator of matrix A in equation (12), denoted by \hat{A} . For one additional case in borough i , denoted by vector e_i in which only the i -th element equals one and all other elements equal zero. This case remains contagious for L periods by assumption. The total (expected) number of new cases created directly by e_i can be estimated as $\sum_{\ell=0}^{L-1} \exp(-\hat{\rho}\ell) \hat{A} e_i$. This quantity above is uniformly bounded by $\sum_{\ell=0}^L \exp(-\hat{\rho}\ell) \sigma_{\max}(\hat{A})$ because $\|e_i\| = 1$, in which $\sigma_{\max}(\cdot)$ represents the function that computes the largest singular value of a matrix. Thus, we have an upper bound for the estimates

of R_0 as follows:

$$\widehat{R}_0 \leq \max_{i \in \{1, \dots, n\}} \left\{ \sum_{\ell=0}^{L-1} \exp(-\widehat{\rho}\ell) \widehat{A} e_i \right\} \leq \sum_{\ell=0}^L \exp(-\widehat{\rho}\ell) \sigma_{\max}(\widehat{A}).$$

Estimates of (upper bounds of) R_0 are presented in Table 5. According to our specification in Section 1.3, we have separate estimates of \widehat{A} before and after the lockdown policy. Thus, the table shows the largest singular values and R_0 s both before and after the policy date. The disease R_0 is around 1.5 before the lockdown policy and is around 0.9 afterwards based on our benchmark specification of incorporating work-to-home and home-to-work networks (last two columns of Table 5). The magnitude of reduction is large though statistically insignificant. This reduction is due to the impacts of lockdown policies on both the autoregressive and network effects.

3.3 The network impulse response functions

To further understand how innovations in daily new COVID-19 cases propagate through networks, we define and calculate the network impulse response function (NIRF) of our model motivated by the analysis in Denbee, Julliard, Li, and Yuan (2021). For a unitary shock (or change in levels) of disease incidents in borough i , its impact on the expected total number of cases across *all* locations τ -period ahead is measured by

$$\text{NIRF}_i(\tau) = \sum_{j=1}^n \frac{\partial \mathbb{E}[y_{j,t+\tau} | \mathcal{F}_t]}{\partial y_{it}}. \quad (19)$$

The empirical model we work with allows an analytical formula for the NIRF, as detailed in Section B of the Appendix.

Plots in Figure 6 illustrate NIRFs across each borough for the time horizon of one week, that is $\tau = 7$. Panel (A) shows the impulse responses before the lockdown. The Westminster/City of London subpopulation strongly dominates all other London boroughs. For one additional case that emerges in this area, three more cases are expected to occur in the whole Greater London area, even after one week. This identifies the Westminster/City of London area as a “key player” for shock propagations through the network in the language of Denbee, Julliard, Li, and Yuan (2021). Camden, Tower Hamlets, Southwark, as well as Lambeth are among the other key players that appear to show strong network impulse responses, but the magnitude is much weaker than for Westminster/City of London. Panel (B) presents results after the lockdown. It offers another angle for us to understand the effectiveness of the lockdown policy, as there is a distinct reduction in the NIRF measure for the key areas such as Westminster/City of London and other boroughs.

Analysing network impulse responses is valuable for designing “smart” partial lockdown

policies that selectively lockdown a few regions instead of deploying a full-scale lockdown. When prescribing a partial lockdown plan, the conventional wisdom is to shutdown areas that have witnessed the largest number of existing cases and are undergoing rapid growth in new cases.¹⁸ Our network impulse response analysis offers another perspective. In addition to focusing on regions that have reported severe outbreaks, lockdown policies should also target areas that are key to the disease transmission. Isolating subpopulations that are key players in the network can forestall rapid spread among the whole population, even if few cases have occurred in these areas. Optimal (partial) lockdown policies should combine both perspectives, as we demonstrate in our counterfactual analysis in the next session.

4 Counterfactual Simulations

This section presents simulations to evaluate counterfactual outcomes from alternative policy interventions. We start by investigating the impacts of earlier or later nation-wide lockdown measures, and compare them with actual numbers. We then compute optimal partial lockdown arrangements and their potential outcomes. We emphasise on comparing optimal policies with “naive” policies that only target areas with the largest number of existing cases. Our goal when making these comparisons is to illustrate the importance of shutting down pivotal nodes of the network as a preventive measure against disease transmission.

4.1 Alternative dates for nationwide lockdown

The UK government implemented a nationwide lockdown on March 23. The timing of this policy has been under intense public scrutiny. Dr. Neil Ferguson who, with his research group's "Imperial College" model, has facilitated the lockdown decision of the UK government said:

“Had we introduced lockdown measures a week earlier, we would have reduced the final death toll by at least a half.” (BBC News, June 10, 2020)

Similar arguments have been made by scientists such as Dr. James Annan and Dr. Kit Yates.¹⁹ In the meantime, Dr. Yates has acknowledged that

"There had been an 'overreliance' on certain models when determining how fast the

¹⁸See, for example, the lockdown of Hubei province in China and Lombardy region in Italy, both of which were the epicentres of COVID-19 outbreaks when the policies came out.

¹⁹These proponents have been broadly covered by the media. James Annan's conclusion was drawn upon his calculation made public on May 12, 2020 through a blog post, which is available at <https://bskiesresearch.wordpress.com/2020/05/12/the-human-cost-of-delaying-lockdown/>. Citing James Annan's calculation, Kit Yates wrote "locking-down a week earlier translates to beginning lockdown with roughly a quarter of the total cases..." in an essay to HuffPost on May 22, 2020. Details can be found at https://www.huffingtonpost.co.uk/entry/lockdown-uk-deaths_uk_5ec6efd8c5b68038a74a50ad?utm_hp_ref=uk-opinion.

epidemic had been doubling; ...that some of the modelling groups had more influence over the consensus decisions than others.” (BBC News, June 10, 2020)

We attempt the same inspection using our model, although within a limited scope, by only focusing on the case of London. With our estimates, we change the policy indicator D_t by allowing for different policy intervention dates and simulate the model outcomes. Specifically, we base simulation exercises on parameter estimates from the benchmark specification (work-to-home and home-to-work networks) reported in Table 1. We consider policy dates two weeks or one week, both before and after March 23. We simulate each of the resulting models 10,000 times and then average the 10,000 paths of daily case counts across all London boroughs as our counterfactual outcomes. Throughout our simulations, we fix the endemic terms, although this element of the model, by definition, is also affected by the specific date of the policy due to variables such as $t \times D_t$ and $t^2 \times D_t$. Under this simulation design, we are indeed treating the endemic term as a deterministic force in the model. The endemic effects are introduced only to isolate the autoregressive and network effects through controlling for variations that are not epidemic.

Simulation results are presented in Figure 7. Plots in this figure show the cumulative number of all London cases from March 1 to June 4. The plot on the left panel compares the simulated outcomes from locking-down one or two weeks earlier with the actual outcome. Based on our results, locking down two weeks earlier translates into a reduction of 20% total cases (5,876 cases on the absolute level) in London during the period under study. The number is 16% (4,385 on the absolute level) if lockdown would have been one week earlier. These numbers indicate that, at least for London, positive action earlier than the March 23 lockdown dates would have yielded reduction in total cases, while the magnitude is not surprisingly large.

The right panel plots alternative situations in which lockdown takes place one or two weeks later. Delaying the March 23 lockdown would cause serious consequences in terms of a large increase in the number of people infected. If the lockdown would have happened one week later, the total number of infected cases up till June 4 would have increased by 37% (10,021 on the absolute level). Postponing the lockdown for two weeks would have led to an much larger increase of over 180%, that is, around fifty thousand more people in London would have been infected. The simulation result indicates that the week from March 30-April 6 could have witnessed an explosive spread of COVID-19 in London were there no public policy interventions early on.

4.2 Optimal partial lockdowns

This section discusses optimal lockdown policies, where by “lockdown” we mean the work-from-home requirements put in place by the UK government. With the parameter estimates

for our network SIR model, we are able to map out the dynamics of COVID-19 spread across London boroughs. This knowledge makes it possible for us to answer the following question: at any given time, what is the optimal borough-specific lockdown scheme that can minimise the number of infected cases in the future? For clarification, our definition of optimality is a constraint on the number of boroughs being locked down. That is, we are searching for optimal solutions to problems such as: “If work-from-home requirements were to be imposed on only three (work location) London boroughs for controlling the spread, which ones are they?”

To address these types of questions, we simulate the dynamics of COVID-19 transmission in London based on parameter estimates of the benchmark in Table 1. We then consider policies that impose the work-from-home restrictions on different combinations of London boroughs (as work locations) on the exact same date of the actual nationwide lockdown, March 23. A total of 10,000 paths of disease case counts is generated from simulations. For each path, we evaluate potential outcomes of all possible partial lockdown policies. For example, if two out of the 32 London boroughs are allowed to be locked down, we then have $\binom{32}{2} = 496$ different lockdown designs. For each policy, the outcome we focus on are the total number of COVID-19 infections in London, averaged across all simulations.

The effects of locking down a particular borough (in the sense of imposing the work-from-home restrictions, and its exceptions, on the workers of that borough) are quantified in two ways. The first relies on the information from our estimates to quantify the impacts of lockdown policies. Under this setting, for boroughs that are locked down, corresponding columns and rows of matrix $W^{(1)}$ and $W^{(2)}$ are downscaled to 63.6% and 18.2% of their original values, respectively.²⁰ Both ways of evaluating lockdown plans ignore the impact on the autoregressive and endemic effects. Hence, the resulting outcomes are conservative when compared with the actual numbers (which can be regarded as direct outcomes due to the March 23 nationwide lockdown that have changed the dynamics of all three effects).

The second “targeted lockdown” policy considers local work-from-home restrictions effectiveness as directly measured by local activity. This is motivated by the fact that our network effects highlight the transmission through commuting between residences and workplaces. We measure the impacts of work-from-home regulations using Google’s COVID-19 Community Mobility Reports. The Google mobility measures are constructed from cell phone tracking data and also used by Farboodi et al. (2021) and Chernozhukov et al. (2021) to calibrate reductions in social activities due to policy restrictions. Based on these data, we can measure the reduction in workplace activities for each London borough after the March 23 Lockdown, tabulated in Table A7 of the Appendix. When investigating the effect of imposing work-from-home restrictions on the workers of a specific borough, we reduce its network effects introduced by

²⁰The relevant quantities here are $\exp(\phi^{(1)}) = 0.636$ and $\exp(\phi^{(2)}) = 0.182$ for the benchmark specification in Table 1 (column 5).

$W^{(1)}$ and $W^{(2)}$ by downscaling their rows and columns using the ratios presented in Table A7.

We start with the simplest case of lockdown policy: work-from-home restrictions are imposed on the workers of only one borough. Simulation results are presented in Figure 8. The top panel uses parameters from our estimation results as described above. The bottom panel (three plots) considers targeted lockdown policies mimicking the work-from-home restrictions effectiveness using Google mobility data. Across all figures, the red line represents the cumulative case numbers across time if there are no lockdown policies implemented at all. The blue line shows the real number. Outcomes from different lockdown plans are marked in grey. We highlight the policy of imposing the work-from-home requirement on only one borough with the highest cumulative number of infected cases (the borough of Lambeth) on the policy date (March 23) in orange. This type of case-targeting policy reflects the conventional wisdom. For comparison, we characterise the optimal policy in pink. This policy is optimal in the sense that it minimises the total (expected) number of infected cases. In our analysis, the optimal single-borough lockdown plan is to impose the work-from-home requirement on workers of Westminster/City of London, which features the largest network impulse responses as shown in Figure 6. The results confirm that lockdown plans which only pay attention to the current number of infected cases are far from optimal (by comparing the orange and pink lines). Instead, imposing the work-from-home restriction on the region that is pivotal for the network propagation of shocks brings major improvements: a reduction of over 20,000 total cases in London.

We proceed to consider the case of imposing work-from-home restrictions on two or three boroughs. Results are shown in Figures 9. The optimal arrangement of locking down two boroughs is to pick Westminster/City of London and Southwark, outcomes of which are shown in pink lines. Up till the date of March 23, the top two boroughs that have witnessed the most severe outbreak are Lambeth and Southwark. Locking down these two boroughs gives rise to outcomes shown in orange in the figures of Panel (A). We can observe again that the optimal lockdown policy of targeting Westminster/City of London and Southwark leads to major improvements over the policy that only targets regions with the largest existing number of cases. It is noteworthy mentioning that the two boroughs with the highest NIRFs are Westminster/City of London and Camden (see Figure 6 for a list of NIRFs). Therefore, we find that the optimal lockdown policy is a combination of two targets: the highest number of COVID-19 cases (the inclusion of Southwark) and the largest NIRFs (the inclusion of Westminster/City of London). Both targets are essential for the design of optimal lockdown policies.

Similar findings appear in Panel (B) of Figure 9 when investigating polices that lockdown three boroughs down. The optimal policy dictates imposing the work-from-home restrictions on Westminster/City of London, Southwark, and Camden. By comparison, the top three boroughs that have been most harshly hit by the pandemic up till March 23 are Lambeth, Southwark, and Brent. It is also worthwhile noting that the top three boroughs with the largest

NIRFs are Westminster/City of London, Camden, and Tower Hamlets, according to Figure 6. One borough, Southwark, out of large-case-count category is again included to the optimal policy. The top two boroughs in terms of NIRFs, Westminster/City of London and Camden, are also crucial for the design of optimal partial lockdown policy.

Our simulations show that the partial lockdown plans are powerful substitutes for full-scale lockdown. Suppose we quantify the impacts of locking down boroughs using the numbers we estimated for the nationwide one. In that case, the optimal three-borough lockdown plan leads to similar outcomes compared with the actual nationwide lockdown (94.6% efficacy). For partial lockdown plans implemented by forbidding people from going to the target boroughs to work, the reduction in total case counts from targeting three boroughs is around 91.5% of the reduction due to the actual nationwide lockdown. We would like to point out that all comparisons above are relatively conservative because we ignore the potential changes these plans can bring to the autoregressive and endemic components.

5 Conclusions

In this paper, we present and estimate a network-SIR model of the spreading of COVID-19 disease in London. Our estimates show that network play a major role in transmitting COVID-19 disease and they cannot be ignored. Based on the estimated epidemic dynamics, we investigate whether a certain target lockdown policy could contain the spread of COVID-19 disease as much as the full scale lockdown and, hence, have a lower economic cost. Our simulations show that an optimal lockdown should target areas that not only have the highest number of existing case, but also those that play a key role in transmitting disease in the contact network among the population. In our case, the contact network corresponds to the commuting network in London. In designing a lockdown policy, our finding calls for special attention to be focused on the network role of the COVID-19 transmission. These network could be train or flight networks, or any other traffic networks at the national or international level including the migration network (from hard-hit COVID-19 hotspots) identified by [Coven, Gupta, and Yao \(2022\)](#). As networks potentially connect regions with different jurisdictional governments, our finding indicates that coordinated regional quarantine and lockdown policies are essential in containing the spread of the COVID-19 pandemic, a conclusion echoed in [Chandrasekhar, Goldsmith-Pinkham, Jackson, and Thau \(2021\)](#).

References

- Acemoglu, D., V. Chernozhukov, I. Werning, and M. D. Whinston (2021). Optimal targeted lockdowns in a multi-group SIR model. *American Economic Review: Insights* 3(4), 487–502.
- Alvarez, F., D. Argente, and F. Lippi (2021). A simple planning problem for COVID-19 lock-down, testing, and tracing. *American Economic Review: Insights* 3(3), 367–82.
- Avery, C., W. Bossert, A. Clark, G. Ellison, and S. F. Ellison (2020). An economist’s guide to epidemiology models of infectious disease. *Journal of Economic Perspectives* 34(4), 79–104.
- Ballester, C., A. Calvó-Armengol, and Y. Zenou (2006). Who’s who in networks. wanted: The key player. *Econometrica* 74(5), 1403–1417.
- Berndt, E. R., B. H. Hall, R. E. Hall, and J. A. Hausman (1974). Estimation and inference in nonlinear structural models. *Annals of Economic and Social Measurement* 3(4), 653–665.
- Chandrasekhar, A. G., P. Goldsmith-Pinkham, M. O. Jackson, and S. Thau (2021). Interacting regional policies in containing a disease. *Proceedings of the National Academy of Sciences* 118(19), e2021520118.
- Chernozhukov, V., H. Kasahara, and P. Schrimpf (2021). Causal impact of masks, policies, behavior on early COVID-19 pandemic in the u.s. *Journal of Econometrics* 220(1), 23–62. Pandemic Econometrics.
- Coven, J., A. Gupta, and I. Yao (2022). JUE Insight: Urban flight seeded the COVID-19 pandemic across the united states. *Journal of Urban Economics*, 103489.
- Denbee, E., C. Julliard, Y. Li, and K. Yuan (2021). Network risk and key players: A structural analysis of interbank liquidity. *Journal of Financial Economics* 141(3), 831–859.
- Easley, D. and J. Kleinberg (2010). *Networks, Crowds, and Markets: Reasoning about a Highly Connected World*. Cambridge University Press.
- Eichenbaum, M. S., S. Rebelo, and M. Trabandt (2021). The macroeconomics of epidemics. *Review of Financial Studies* 34(11), 5149–5187.
- Farboodi, M., G. Jarosch, and R. Shimer (2021). Internal and external effects of social distancing in a pandemic. *Journal of Economic Theory* 196, 105293.
- Fernández-Villaverde, J. and C. I. Jones (2022). Estimating and simulating a SIRD model of COVID-19 for many countries, states, and cities. *Journal of Economic Dynamics and Control*, 104318.
- Finkenstädt, B. F. and B. T. Grenfell (2000). Time series modelling of childhood diseases: a dynamical systems approach. *Journal of the Royal Statistical Society: Series C* 49(2), 187–205.
- Garriga, C., R. Manuelli, and S. Sanghi (2022). Optimal management of an epidemic: Lockdown, vaccine and value of life. *Journal of Economic Dynamics and Control* 140, 104351. Covid-19 Economics.
- Gollier, C. (2020). Cost–benefit analysis of age-specific deconfinement strategies. *Journal of Public Economic Theory* 22(6), 1746–1771.
- Grimmett, G. R. and D. R. Stirzaker (2001). *Probability and Random Processes (Third Edition)*. Oxford University Press.
- Held, L., M. Höhle, and M. Hofmann (2005). A statistical framework for the analysis of multivariate infectious disease surveillance counts. *Statistical Modelling* 5(3), 187–199.
- Jackson, M. O. (2008). *Social and Economic Networks*. Princeton University Press.
- Jones, C., T. Philippon, and V. Venkateswaran (2021). Optimal mitigation policies in a pandemic: Social distancing and working from home. *Review of Financial Studies* 34(11), 5188–5223.
- Kermack, W. O. and A. G. McKendrick (1927). A contribution to the mathematical theory of epidemics. *Proceedings of the Royal Society of London. Series A* 115(772), 700–721.

- Lawson, A. B. (2013). *Bayesian Disease Mapping: Hierarchical Modeling in Spatial Epidemiology*. CRC press.
- Lee, S., Y. Liao, M. H. Seo, and Y. Shin (2021). Sparse hp filter: Finding kinks in the COVID-19 contact rate. *Journal of Econometrics* 220(1), 158–180. Pandemic Econometrics.
- Li, S. and O. Linton (2021). When will the COVID-19 pandemic peak? *Journal of Econometrics* 220(1), 130–157. Pandemic Econometrics.
- Liu, L., H. R. Moon, and F. Schorfheide (2021). Panel forecasts of country-level COVID-19 infections. *Journal of Econometrics* 220(1), 2–22. Pandemic Econometrics.
- Newman, M. E. (2002). Spread of epidemic disease on networks. *Physical review E* 66(1), 016128.

Table 1: Estimation results of the Network-SIR model of Section 1.3. Results in columns (1)-(3) correspond, respectively, to specifications with only one of the following transmission networks: “work-to-home”, “home-to-work”, and “home-to-home”. Column (1,2,3) include all the three networks while column (1,2) uses only the first two networks.

Model \mathcal{G}	(1)		(2)		(3)		(1,2,3)		(1,2)	
Value	est.	se.	est.	se.	est.	se.	est.	se.	est.	se.
Autoregressive effect										
$\exp(\gamma_0)$	0.376	0.033	0.456	0.033	0.419	0.031	0.340	0.037	0.341	0.037
$\exp(\gamma)$	0.470	0.050	0.514	0.044	0.462	0.043	0.527	0.066	0.522	0.065
Network effect										
$\mathbf{W}^{(1)} = K:$										
$\exp\left(\phi_0^{(1)}\right)$	0.556	0.065					0.581	0.070	0.582	0.069
$\exp\left(\phi^{(1)}\right)$	0.785	0.103					0.569	0.088	0.636	0.102
$\mathbf{W}^{(2)} = K^\top:$										
$\exp\left(\phi_0^{(2)}\right)$			0.073	0.021			0.045	0.019	0.039	0.020
$\exp\left(\phi^{(2)}\right)$			0.606	0.181			0.750	0.331	0.182	0.427
$\mathbf{W}^{(3)} = KK^\top:$										
$\exp\left(\phi_0^{(3)}\right)$					0.278	0.035	0.000	0.000		
$\exp\left(\phi^{(3)}\right)$					0.604	0.081	0.000	0.000		
pseudo- R^2	81.8%		80.9%		81.4%		81.9%		81.9%	
# obs.	3008		3008		3008		3008		3008	

Table 2: Estimation results of the Network-SIR model of Section 1.3 adding day fixed effects. Results in columns (1)-(3) correspond, respectively, to specifications with only one of the following transmission networks: “work-to-home;” “home-to-work;” “home-to-home”. Column (1,2,3) considers the three networks jointly while column (1,2) uses only the first two networks.

Model \mathcal{G}	(1)		(2)		(3)		(1,2,3)		(1,2)	
Value	est.	se.	est.	se.	est.	se.	est.	se.	est.	se.
Autoregressive effect										
$\exp(\gamma_0)$	0.313	0.032	0.302	0.025	0.291	0.033	0.269	0.034	0.269	0.034
$\exp(\gamma)$	0.402	0.059	0.419	0.043	0.428	0.060	0.467	0.077	0.467	0.077
Network effect										
$\mathbf{W}^{(1)} = K$										
$\exp\left(\phi_0^{(1)}\right)$	0.286	0.050					0.275	0.053	0.275	0.053
$\exp\left(\phi^{(1)}\right)$	0.326	0.138					0.324	0.144	0.324	0.144
$\mathbf{W}^{(2)} = K^\top$										
$\exp\left(\phi_0^{(2)}\right)$			0.080	0.029			0.065	0.030	0.065	0.030
$\exp\left(\phi^{(2)}\right)$			0.000	0.000			0.000	0.000	0.000	0.000
$\mathbf{W}^{(3)} = KK^\top$										
$\exp\left(\phi_0^{(3)}\right)$					0.152	0.032	0.000	0.000		
$\exp\left(\phi^{(3)}\right)$					0.000	0.000	0.146	0.000		
pseudo- R^2	85.9%		86.0%		85.9%		85.9%		85.9%	
# obs.	3008		3008		3008		3008		3008	

Table 3: Estimation of the Network-SIR model in Section 1.3. Results in columns (1)-(3) correspond, respectively, to specifications with only one of the following transmission networks: (i) only diagonal proportional to the fraction of population, (ii) having equal off-diagonal elements (compound symmetric), (iii) off-diagonals are determined only by distances between centroids of boroughs, transformed by a square exponential kernel $\kappa(d) = \exp(-100d^2)/10$. Column (1,2,3) considers the three networks jointly while column (1,2) uses only the first two networks. ΔAIC represents the difference between the Akaike information criteria of the estimated models and our preferred model (1,2) estimated using commuting networks.

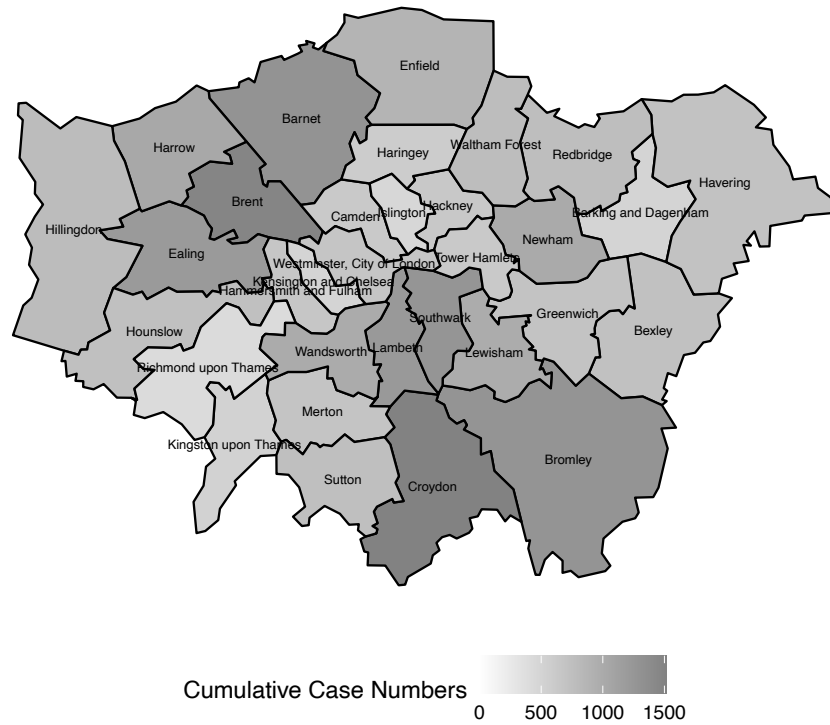
Model \mathcal{G}	(1)		(2)		(3)		(1,2,3)	
Value	est.	se.	est.	se.	est.	se.	est.	se.
Autoregressive effect								
$\exp(\gamma_0)$	0.483	0.077	0.370	0.033	0.569	0.021	0.331	0.083
$\exp(\gamma)$	0.435	0.090	0.539	0.055	0.339	0.022	0.516	0.144
Network effect								
$W^{(1)}$: diagonal								
$\exp\left(\phi_0^{(1)}\right)$	1.000	2.223					1.000	2.711
$\exp\left(\phi^{(1)}\right)$	1.000	2.161					1.000	2.685
$W^{(2)}$: compound symmetric								
$\exp\left(\phi_0^{(2)}\right)$			0.409	0.062			0.415	0.066
$\exp\left(\phi^{(2)}\right)$			0.973	0.151			0.975	0.159
$W^{(3)}$: square exponential kernel								
$\exp\left(\phi_0^{(3)}\right)$					0.341	0.058	0.000	0.026
$\exp\left(\phi^{(3)}\right)$					0.939	0.173	0.939	5.991
ΔAIC	221.5		115.5		94.1		116.1	
# obs.	3008		3008		3008		3008	

Table 4: Estimation of the Network-SIR model in Section 1.3. Results in the first three columns correspond, respectively, to specifications of adding one of the following transmission networks: (i) only diagonal proportional to the fraction of population, (ii) having equal off-diagonal elements (compound symmetric), (iii) off-diagonals are determined only by distances between centroids of boroughs, transformed by a square exponential kernel $\kappa(d) = \exp(-100d^2)/10$, to our work-to-home and home-to-work commuting networks. For comparison, the fourth column reports estimates including only the two commuting networks (which repeats the last column of Table 1). ΔAIC represents the difference between the Akaike information criteria of any one of the first three models and the last model.

Model \mathcal{G}	(1,2, diag.)		(1,2, c.s.)		(1,2, s.k.)		(1,2)	
Value	est.	se.	est.	se.	est.	se.	est.	se.
Autoregressive effect								
$\exp(\gamma_0)$	0.305	0.073	0.366	0.036	0.342	0.037	0.341	0.037
$\exp(\gamma)$	0.578	0.172	0.483	0.056	0.517	0.065	0.522	0.065
Network effect								
$W^{(1)} = K$:								
$\exp(\phi_0^{(1)})$	0.591	0.070	0.425	0.090	0.560	0.079	0.582	0.069
$\exp(\phi^{(1)})$	0.843	0.107	0.489	0.194	0.709	0.136	0.636	0.102
$W^{(2)} = K^\top$:								
$\exp(\phi_0^{(2)})$	0.041	0.021	0.000	0.017	0.036	0.021	0.039	0.020
$\exp(\phi^{(2)})$	0.000	0.000	0.000	0.000	0.000	0.000	0.182	0.427
$W^{(3)}$: diagonal / compound symmetric / square exponential kernel								
$\exp(\phi_0^{(3)})$	1.000	1.946	0.189	0.089	0.044	0.076		
$\exp(\phi^{(3)})$	0.015	1.036	1.000	0.558	1.000	2.052		
pseudo- R^2	81.8%		81.9%		81.9%		81.9%	
ΔAIC	24.7		7.7		9.7			
# obs.	3008		3008		3008		3008	

Table 5: Estimation-implied upper bound for the basic reproduction number R_0 of COVID-19 in London. σ_{\max} denotes the largest singular value of the estimated matrix A in equation (15).

Model \mathcal{G}	(1)		(2)		(3)		(1,2,3)		(1,2)	
Value	est.	se.	est.	se.	est.	se.	est.	se.	est.	se.
Before Lockdown Policy: $D_t = 0$										
σ_{\max}	0.830	0.582	0.509	0.103	0.632	0.285	0.842	0.573	0.841	0.582
R_0	1.508	1.057	0.924	0.187	1.147	0.517	1.529	1.041	1.528	1.056
After Lockdown Policy: $D_t = 1$										
σ_{\max}	0.550	0.416	0.267	0.037	0.324	0.144	0.470	0.314	0.493	0.349
R_0	0.999	0.755	0.485	0.068	0.589	0.262	0.854	0.570	0.896	0.634



(A) COVID-19 cases for boroughs in London (up till June 4, 2020)



(B) Population sizes for boroughs in London (year 2020)

Figure 1: Summary statistics: cumulative number of cases (panel A) and subpopulation sizes (panel (B)).

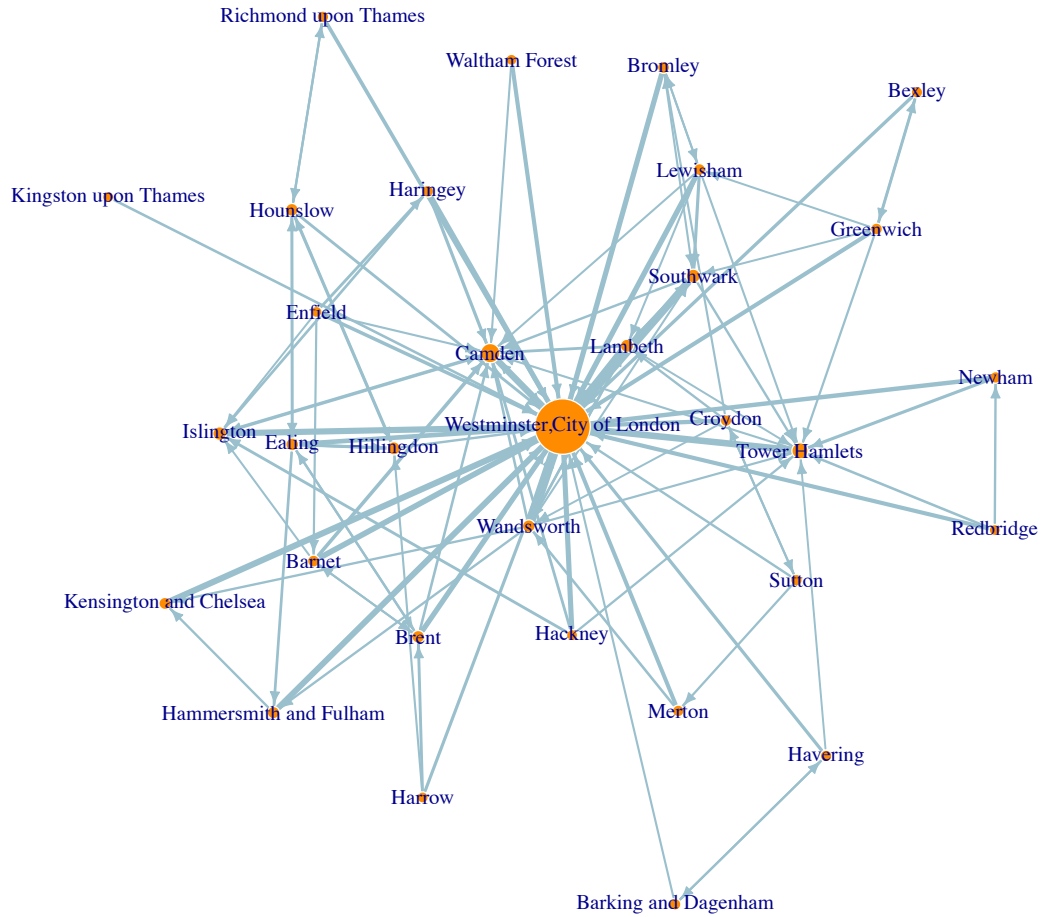
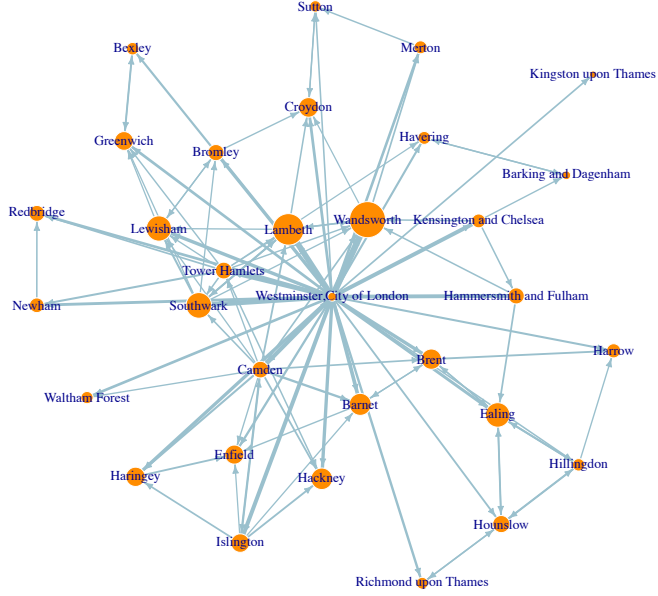
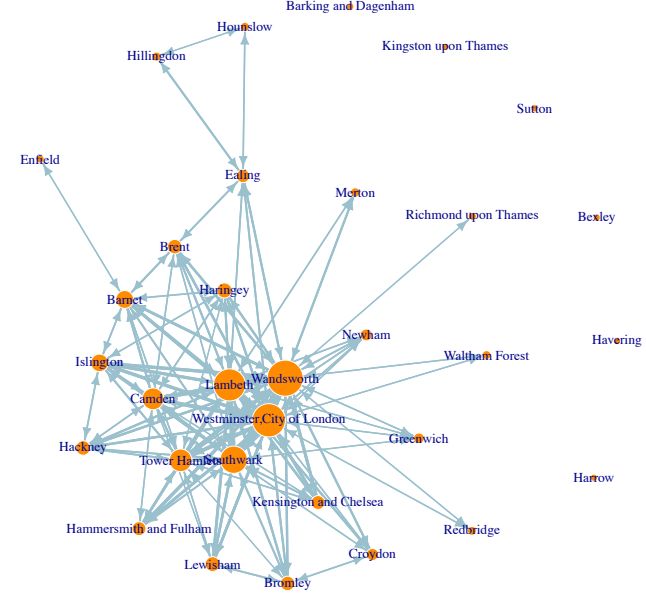


Figure 2: The graph of network $W^{(1)} = K$. This network is constructed using 2011 UK census data. Nodes represent London boroughs. Node sizes are proportional to their total in-degrees. Directed edges represent the amount of people going to work from one borough to another. Edge widths are proportional to their respective values in the graph. Only edges which exceed the 80% percentile are drawn.



(A) Graph of $W^{(2)}$: defined by adjacency matrix K^\top



(B) Graph of $W^{(3)}$: defined by adjacency matrix KK^\top

Figure 3: Graphs of network $W^{(2)}$ and $W^{(3)}$. Both networks are constructed based on network $W^{(1)} = K$ shown in Figure 2. Nodes represent London boroughs. Node sizes are proportional to their total in-degrees. Edge widths are proportional to their respective values in the graph. Only edges which exceed the 80% percentile are drawn.

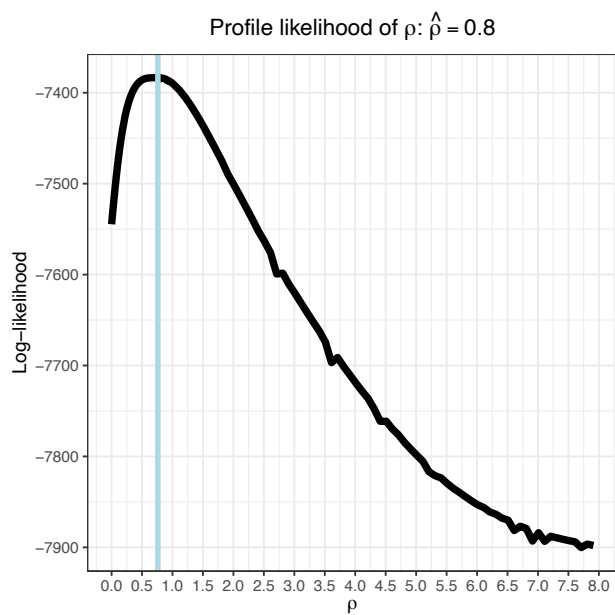
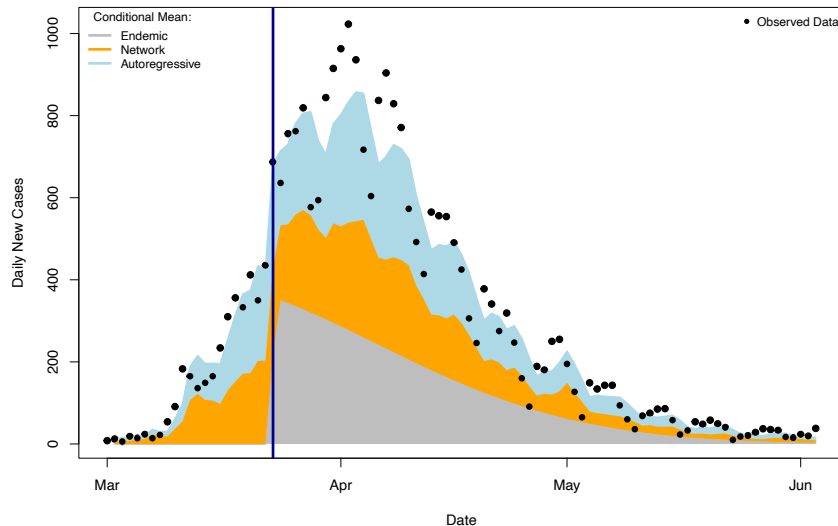
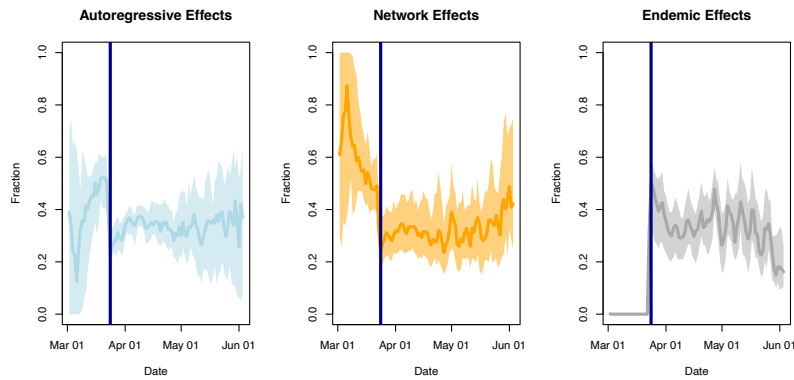


Figure 4: Tuning parameter ρ for the decaying function $\nu(\ell) = \exp(-\rho\ell)$ determining the actively infectious population.



(A) Decomposition of total (expected) daily new cases in London across time

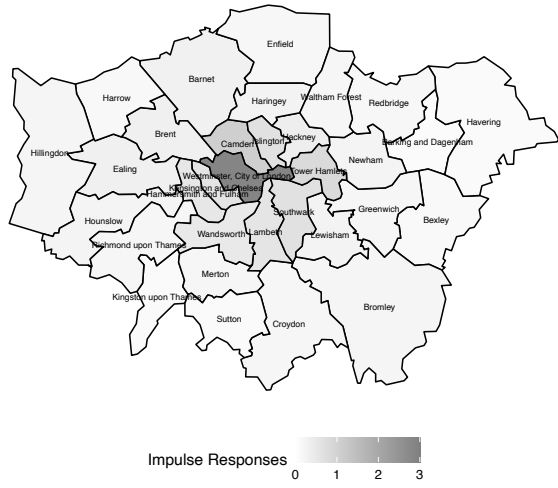


(B) The autoregressive, (total) network, and endemic effects as fractions: μ_{it}^{AR} / μ_{it} , μ_{it}^{NE} / μ_{it} , μ_{it}^{EN} / μ_{it}

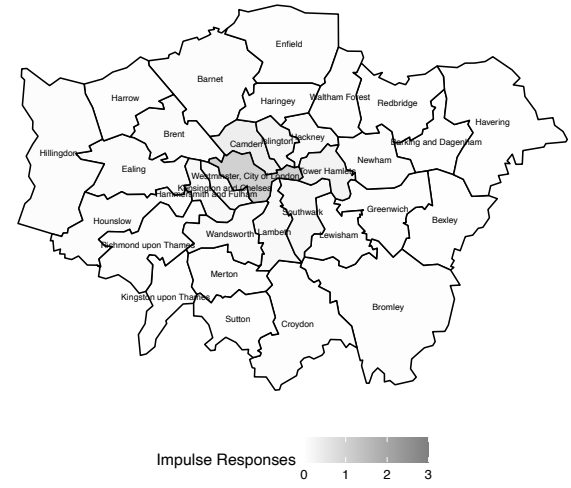
(C) The two network effects as fractions: $\mu_{it}^{NE,(g)} / \mu_{it}$, $g \in \{1, 2\}$

Figure 5: Decomposition of the conditional mean: total daily new cases in London. Effects in Panel (A) are based on summing across all London boroughs. Bands in Panel (B) are 10% to 90% percentiles across all London boroughs. Solid lines are the median level.

(A) Before lockdown



(B) After lockdown



Borough	Before Lockdown (Impulse Response)	After Lockdown (Impulse Response)
Westminster, City of London	2.857	1.033
Camden	1.077	0.368
Tower Hamlets	0.828	0.269
Islington	0.681	0.212
Southwark	0.662	0.184
Kensington and Chelsea	0.609	0.199
Lambeth	0.585	0.144
Hammersmith and Fulham	0.536	0.164
Wandsworth	0.501	0.108
Hackney	0.389	0.104
Brent	0.341	0.089
Ealing	0.330	0.088
Barnet	0.317	0.072
Haringey	0.266	0.055
Lewisham	0.258	0.048
Hounslow	0.254	0.074
Newham	0.253	0.055
Bromley	0.221	0.037
Hillingdon	0.220	0.066
Merton	0.210	0.044
Croydon	0.209	0.039
Greenwich	0.206	0.039
Richmond upon Thames	0.193	0.046
Waltham Forest	0.191	0.037
Enfield	0.187	0.039
Redbridge	0.168	0.028
Harrow	0.159	0.035
Bexley	0.125	0.020
Kingston upon Thames	0.120	0.026
Havering	0.113	0.018
Sutton	0.111	0.022
Barking and Dagenham	0.093	0.018

Figure 6: Network impulse response functions (one-week horizon), from equation (19), before (panel (A)), and after (panel (B)), lockdown.

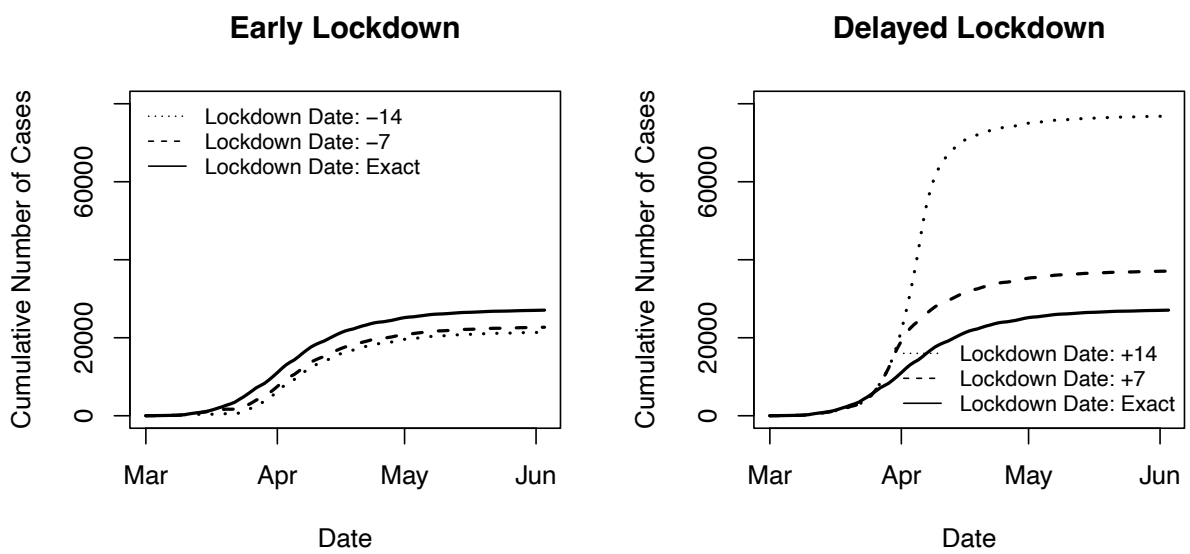
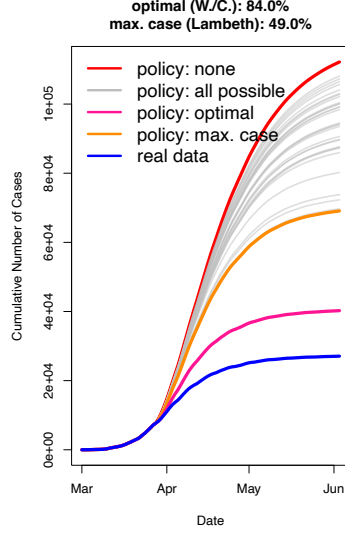


Figure 7: Cumulated number of cases over time (continuous black line) and counterfactual cumulated number of cases with earlier (left figure) and later (right figure) lockdown time.

(A) Partial lockdown policies based on our estimated effects (one borough)



(B) Borough specific work-from-home enforcement based on Google activity data (one borough)

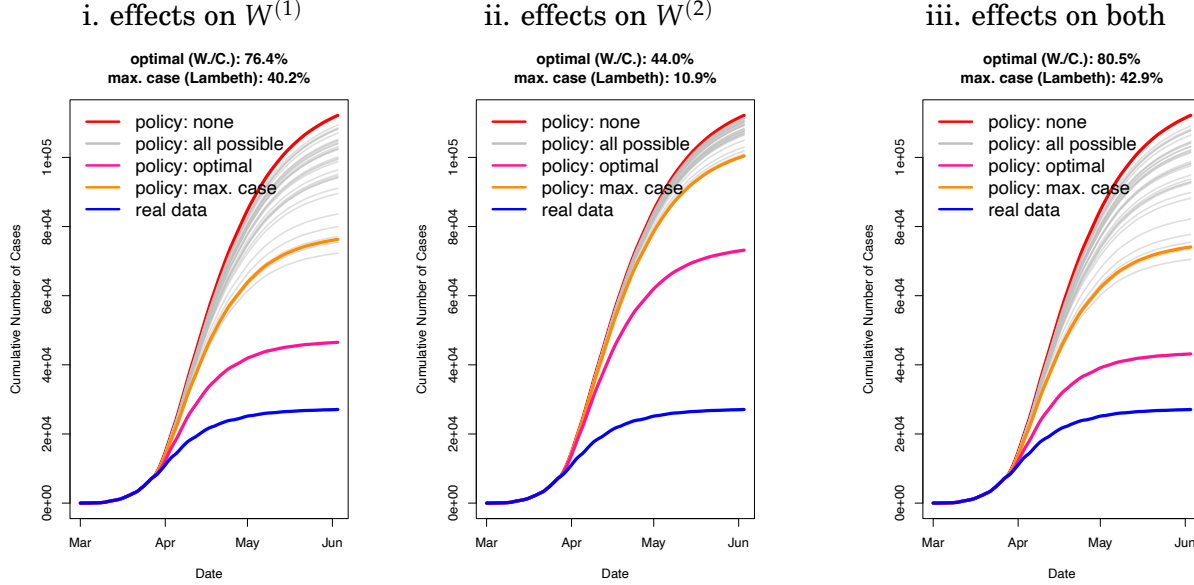


Figure 8: Cumulated number of cases over time with one borough as the policy target: actual (blue line); counterfactual without lockdown (red line); counterfactual with lockdown of only one borough (all cases, grey); counterfactual with lockdown or work-from-home restrictions of only the borough with the most cases (orange line); counterfactual with optimally chosen borough (pink line). On the top panel, the corresponding columns and rows of matrices $W^{(1)}$ and $W^{(2)}$ are downscaled, respectively, to 63.6% and 18.2% of their original values. On the bottom panel, we downscale the network effects using values from Google activity data for each borough according to Table A7, mimicking the results of work-from-home restrictions. W.C. is short for the combined borough Westminster/City of London. The percentage efficacy numbers equal reductions from our simulated partial lockdown policies (red minus pink on June 3rd in the case of optimal policy) divided by reductions from the March 23 nationwide lockdown (red minus blue on June 3rd).

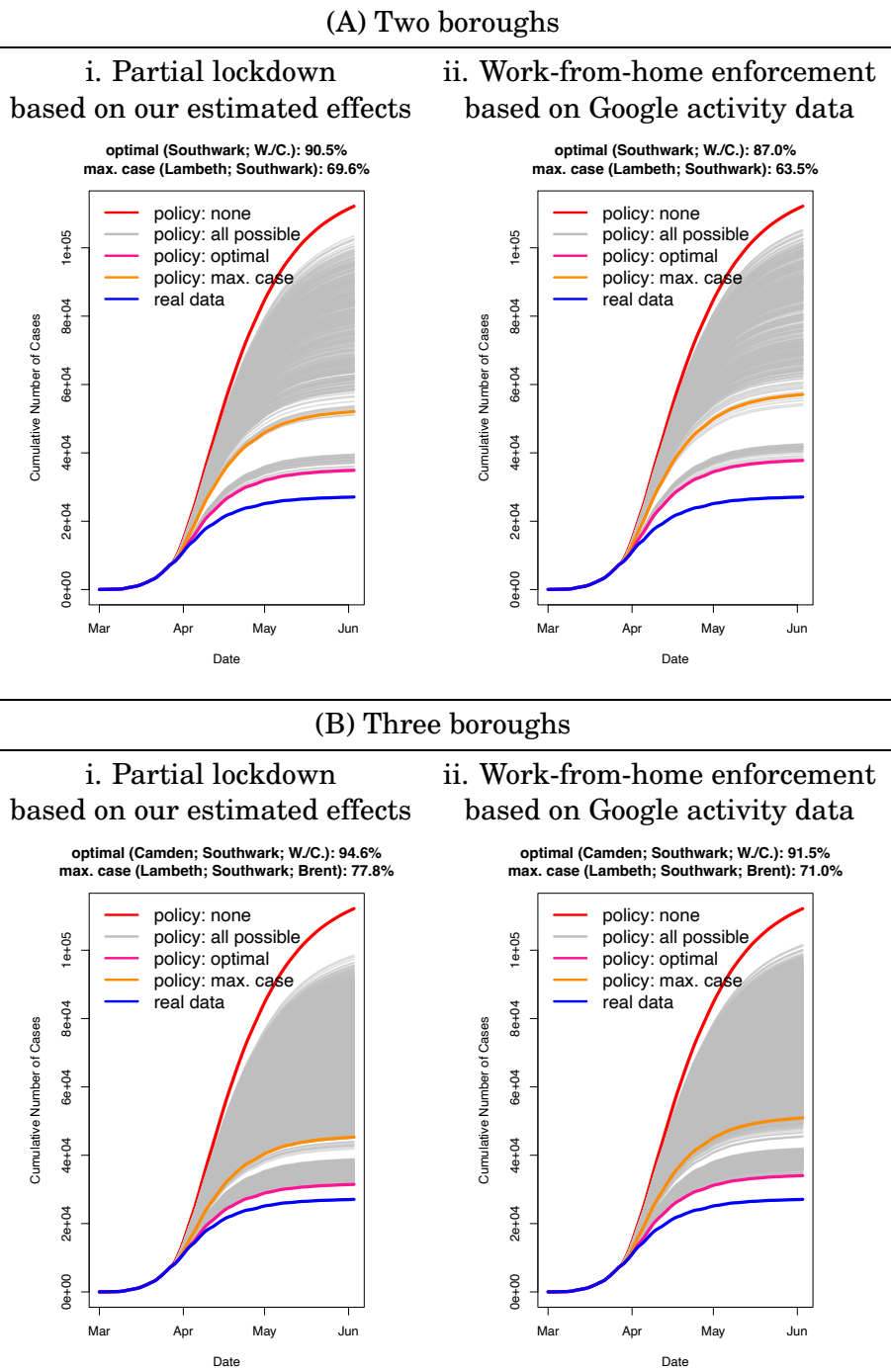


Figure 9: Cumulated number of cases over time with two (Panel A) or three (Panel B) boroughs as the policy target: actual (blue line); counterfactual without lockdown (red line); counterfactual with lockdown of only one borough (all cases, grey); counterfactual with lockdown or work-from-home restrictions of only the borough with the most cases (orange line); counterfactual with optimally chosen borough (pink line). The effects of partially locking down boroughs (figures on the left) is quantified by downscaling corresponding columns and rows of matrices $W^{(1)}$ and $W^{(2)}$ to 63.6% and 18.2% of their original values. The effects of work-from-home restrictions (figures on the right) is captured using values from Google activity data for each borough according to Table A7. W.C. is short for the combined borough Westminster/City of London. The percentage efficacy numbers equal reductions from our simulated partial lockdown policies (red minus pink on June 3rd in the case of optimal policy) divided by reductions from the March 23 nationwide lockdown (red minus blue on June 3rd)

Appendix for “COVID-19 Spread in London: Network Effects and Optimal Lockdowns”

A MLE details

Under a model \mathcal{G} , the log-likelihood function given the observed panel of daily new case numbers Y for parameters $\Theta(\mathcal{G}) = \left\{ \gamma_0, \gamma, \left\{ \phi_0^{(g)} \right\}_{g \in \mathcal{G}}, \left\{ \phi^{(g)} \right\}_{g \in \mathcal{G}}, \beta, \{\eta_i\}_{i=1}^n \right\}$ can be written as

$$\begin{aligned} & \ell(\Theta | Y, \mathcal{G}) \\ &= \sum_{i=1}^n \sum_{t=1}^T \left\{ \log \Gamma(y_{it} + x_{i,t-1}) - \log \Gamma(x_{i,t-1}) - \log \Gamma(y_{it} + 1) \right. \\ & \quad \left. - (x_{i,t-1} + y_{it}) \log(1 + \mu_{it} x_{i,t-1}^{-1}) + y_{it} (\log \mu_{it} + x_{i,t-1}^{-1}) \right\} \end{aligned}$$

where $\Gamma(\cdot)$ is the standard gamma function; μ_{it} is the conditional mean of daily new cases defined as

$$\mu_{it} = \underbrace{\exp(\gamma_0 + D_t \gamma) x_{i,t-1}}_{\mu_{it}^{AR}} + \underbrace{\sum_{g \in \mathcal{G}} \exp(\phi_0^{(g)} + D_t \phi^{(g)}) \left(\sum_{j \neq i} w_{ij}^{(g)} x_{j,t-1} \right)}_{\mu_{it}^{NE,(g)}} + \underbrace{\exp(z_t^\top \beta + \eta_i) N_i}_{\mu_{it}^{EN}}.$$

Taking derivative, we have the following set of score functions:

$$S(\Theta) = \left\{ S_{\gamma_0}, S_\gamma, \left\{ S_{\phi_0^{(g)}} \right\}_{g \in \mathcal{G}}, \left\{ S_{\phi^{(g)}} \right\}_{g \in \mathcal{G}}, S_\beta, \{S_{\eta_i}\}_{i=1}^n \right\}(\Theta)$$

defined as

$$\begin{aligned} S_{\gamma_0}(\Theta) &= \frac{\partial \ell}{\partial \gamma_0} = \sum_{i=1}^n \sum_{t=1}^T \frac{y_{it} - \mu_{it}}{1 + x_{i,t-1}^{-1} \mu_{it}} \frac{\mu_{it}^{AR}}{\mu_{it}}, \quad S_\gamma(\Theta) = \frac{\partial \ell}{\partial \gamma} = \sum_{i=1}^n \sum_{t=1}^T \frac{y_{it} - \mu_{it}}{1 + x_{i,t-1}^{-1} \mu_{it}} \frac{\mu_{it}^{AR}}{\mu_{it}} D_t, \\ S_{\phi_0^{(g)}}(\Theta) &= \frac{\partial \ell}{\partial \phi_0^{(g)}} = \sum_{i=1}^n \sum_{t=1}^T \frac{y_{it} - \mu_{it}}{1 + x_{i,t-1}^{-1} \mu_{it}} \frac{\mu_{it}^{NE,(g)}}{\mu_{it}}, \quad S_{\phi^{(g)}}(\Theta) = \frac{\partial \ell}{\partial \phi^{(g)}} = \sum_{i=1}^n \sum_{t=1}^T \frac{y_{it} - \mu_{it}}{1 + x_{i,t-1}^{-1} \mu_{it}} \frac{\mu_{it}^{NE,(g)}}{\mu_{it}} D_t \end{aligned}$$

for any $g \in \mathcal{G}$, and

$$\begin{aligned} S_\beta(\Theta) &= \frac{\partial \ell}{\partial \beta} = \sum_{i=1}^n \sum_{t=1}^T \frac{y_{it} - \mu_{it}}{1 + x_{i,t-1}^{-1} \mu_{it}} \frac{\mu_{it}^{EN}}{\mu_{it}} z_t, \\ S_{\eta_i}(\Theta) &= \frac{\partial \ell}{\partial \eta_i} = \sum_{t=1}^T \frac{y_{it} - \mu_{it}}{1 + x_{i,t-1}^{-1} \mu_{it}} \frac{\mu_{it}^{EN}}{\mu_{it}} \end{aligned}$$

for each $i = 1, \dots, n$.

Our MLE estimator $\hat{\Theta}$ solves the system of score equations, that is $S(\hat{\Theta}) = 0$. Standard errors are then computed as $\sqrt{\text{diag}(\{S(\hat{\Theta})S(\hat{\Theta})^\top\}^{-1})}$, based on the outer product of score vectors à la [Berndt, Hall, Hall, and Hausman \(1974\)](#).

B Network impulse response function

To compute the NIRFs, we begin from the following fully vectorized representation. Define an $(n \times L)$ -dimension vector $\tilde{\mathbf{y}}_t^\top = [\mathbf{y}_t^\top, \mathbf{y}_{t-1}^\top, \dots, \mathbf{y}_{t-L+1}^\top]^\top$ which concatenates the current and lagged- $(L - 1)$ observations. Then

$$\begin{aligned}\mathbb{E}[\tilde{\mathbf{y}}_{t+1} | \mathcal{F}_t] &= \begin{bmatrix} \mathbf{A}\mathbf{x}_t + \boldsymbol{\mu}_t^{EN} \\ \mathbf{y}_t \\ \mathbf{y}_{t-1} \\ \vdots \\ \mathbf{y}_{t-L+2} \end{bmatrix} \\ &= \begin{bmatrix} \mathbf{A} \sum_{\ell=0}^{L-1} v(\ell) \mathbf{y}_{t-\ell} \\ \mathbf{y}_t \\ \mathbf{y}_{t-1} \\ \vdots \\ \mathbf{y}_{t-L+2} \end{bmatrix} + \begin{bmatrix} \boldsymbol{\mu}_t^{EN} \\ \mathbf{0} \\ \mathbf{0} \\ \vdots \\ \mathbf{0} \end{bmatrix} \\ &= \underbrace{\begin{bmatrix} A\nu(0) & A\nu(1) & \cdots & A\nu(L-2) & A\nu(L-1) \\ I & \mathbf{0} & \cdots & \mathbf{0} & \mathbf{0} \\ \mathbf{0} & I & \cdots & \mathbf{0} & \mathbf{0} \\ \vdots & \vdots & \vdots & \vdots & \vdots \\ \mathbf{0} & \mathbf{0} & \cdots & I & \mathbf{0} \end{bmatrix}}_{\tilde{\mathbf{A}}(L)} \tilde{\mathbf{y}}_t + \begin{bmatrix} \boldsymbol{\mu}_t^{EN} \\ \mathbf{0} \\ \mathbf{0} \\ \vdots \\ \mathbf{0} \end{bmatrix}.\end{aligned}$$

As a result, $\mathbb{E}[\tilde{\mathbf{y}}_{t+\tau} | \mathcal{F}_t] = [\tilde{\mathbf{A}}(L)]^\tau \tilde{\mathbf{y}}_t + \text{const.}$, which implies that

$$\text{NIRF}_{it}(\tau) = \sum_{j=1}^n \frac{\partial \mathbb{E}[y_{j,t+\tau} | \mathcal{F}_t]}{\partial y_{it}} = \sum_{j=1}^n [\tilde{\mathbf{A}}(L)]_{ji}^\tau,$$

where the subscript (ji) of a matrix denotes its element on the j -th row and the i -th column. Estimations of the NIRFs are then calculated through plugging parameter estimates into the expression for matrix A .

C The network SIR model and its estimation when $S_t/N \neq 1$

The stochastic SIR model. Recall that we have derived the negative binomial model for the surveillance counts, that is,

$$y_t \mid \mathcal{F}_{t-1} \sim \text{NegBinom}(p, x_{t-1}),$$

$$p = 1 - \exp(\alpha) \approx 1 - \exp(\theta_I - \theta_R).$$

Under this model, the conditional expectation of y_t is

$$\mathbb{E}[y_t \mid \mathcal{F}_{t-1}] = ax_{t-1} = [\exp(\theta_I - \theta_R) - 1] x_{t-1} \approx (\theta_I - \theta_R)x_{t-1}.$$

Now that we are discarding the assumption that $S_t/N \approx 1$, let $\alpha_t = \theta_I S_t/N - \theta_R$, the model becomes

$$y_t \mid \mathcal{F}_{t-1} \sim \text{NegBinom}(p_{t-1}, x_{t-1}),$$

$$p_{t-1} = 1 - \exp(\alpha_{t-1}) = 1 - \exp\left(\theta_I \frac{S_{t-1}}{N} - \theta_R\right).$$

Of note, here we are still assuming that conditional on the time- $(t-1)$ information \mathcal{F}_{t-1} , α_{t-1} is a constant within the record window h of the surveillance (one day for our data) for simplicity. Under this extension, the conditional expectation of y_t is

$$\mathbb{E}[y_t \mid \mathcal{F}_{t-1}] = a_{t-1}x_{t-1} = \left[\exp\left(\theta_I \frac{S_{t-1}}{N} - \theta_R\right) - 1\right] x_{t-1} \approx \left(\theta_I \frac{S_{t-1}}{N} - \theta_R\right) x_{t-1}.$$

The exact SIR specification basically implies that the conditional mean of newly infected individuals each period changes from $(\theta_I - \theta_R)x_{t-1}$ to $(\theta_I S_{t-1}/N - \theta_R)x_{t-1}$.

The stochastic network SIR model. Now we draw parallel to the network version of our SIR model. Denote by S_{it} and N_i the number of susceptible individuals (at time t) and the number of residents in borough i . Holding the likelihood specification in (11) unchanged, the original conditional mean, assuming $S_{it}/N_i = 1$ for all i , is

$$\mu_t = Ax_{t-1} + \mu_t^{EN} = \left(\gamma I + \sum_{g=1}^G \theta^{(g)} W^{(g)}\right) x_{t-1} + \mu_t^{EN}.$$

A further parameterized matrix A in the sense of single-site SIR can be written as $A = \Theta_I - \Theta_R$, where Θ_I is a matrix determining the transmission rate after the susceptible contract infected ones, Θ_R is a matrix capturing the rate of recovery from time $(t-1)$ to t . There is one key difference between Θ_I and Θ_R : cross-borough network effects are crucial only for transmission. In other words, recovery is independent (across boroughs, or even households). Thus, we can write $\Theta_R = \theta_R I$ (assuming that recovery rates are the same across boroughs).

After dropping the assumption that $S_{it}/N_i = 1$, the constant matrix A is replaced by

$$A_t = \Theta_I S_t - \theta_R I,$$

where $S_t = \text{diag}(S_{1t}/N_1, S_{2t}/N_2, \dots, S_{nt}/N_n)$. Now following equation (15), we specify Θ_I as

$$\Theta_I = \gamma I + \sum_{g=1}^G \theta^{(g)} W^{(g)},$$

the conditional mean vector μ_t now becomes

$$\mu_t = (\Theta_I S_{t-1} - \theta_R I) x_{t-1} + \mu_t^{EN} = \left(\gamma I + \sum_{g=1}^G \theta^{(g)} W^{(g)}\right) S_{t-1} x_{t-1} - \theta_R x_{t-1} + \mu_t^{EN}. \quad (20)$$

We keep the original parameterisation of γ and θ and let $\theta_R = \exp(\phi_R)$ (lockdown policies should not affect the rate of recovery). We estimate the model under this new specification using maximum likelihood.

We tabulate the results of model estimation below. The first two networks are included, which is our preferred specification according to Table 1. The conditional mean vector is specified by equation (20). In the first configuration, we force $\phi_R = -\infty$ (or equivalently, $\theta_R = \exp(\phi_R) = 1$). This specification is equivalent to estimating our original model when x_{t-1} is replaced by $S_t x_{t-1}$, that is, downscaling the actively infective cases by the fraction of

susceptibles in each borough. The second configuration relaxes the restriction. Estimates from the first configuration agree almost perfectly with ones we present in Table 1 (the last two columns incorporating the first two networks), suggesting that time variation of susceptible population across boroughs does not change our empirical results. Under the second configuration, due to the high correlation between $S_t x_t$ and x_t , standard errors increase. Parameter estimates remain largely unchanged. Estimates for the recover rate parameter ϕ_R is 0.068, indicating that the average duration for recovery is around $(1/\phi_R) \approx 15$ days. However, we do not have enough power to conclude that ϕ_R is significantly different from zero.

Table A1: Estimates of the network SIR model without assuming $S_t/N = 1$.

Model \mathcal{G} Value	(1,2)		(1,2)	
	est.	se.	est.	se.
Autoregressive effect				
$\exp(\gamma_0)$	0.338	0.052	0.429	0.237
$\exp(\gamma)$	0.515	0.060	0.510	0.110
Network effect				
$W^{(1)} = K$:				
$\exp(\phi_0^{(1)})$	0.546	0.058	0.659	0.400
$\exp(\phi^{(1)})$	0.698	0.117	0.701	0.179
$W^{(2)} = K^\top$:				
$\exp(\phi_0^{(2)})$	0.044	0.018	0.059	0.079
$\exp(\phi^{(2)})$	0.202	0.489	0.308	0.874
The recovery rate				
$\exp(\phi_R)$			0.068	0.105
pseudo- R^2	82.00%		82.00%	
$\log L$	-7315.89		-7315.59	
p -value for $H_0 : \exp(\phi_R) = 0$, $H_1 : \exp(\phi_R) \neq 0$			0.561	
# obs.	3008		3008	

D The “co-traveling” network between boroughs: the impacts of traveling together

Our goal here is to construct a network quantifying the propensity of residents in borough i and borough j that travel together via the Transport for London (TfL) network.

We rely on the TfL network structure to construct this co-traveling network. Denote by s_1, \dots, s_n the busiest stations of within the TfL network for boroughs $1, \dots, n$. We first find the shortest path between them in the network. Denoted by \mathcal{P}_{ij} the stations on this shortest path in between s_i and s_j . For example, if the shortest path between s_1 and s_2 is $s_1 - s_4 - s_6 - s_2$, then $\mathcal{P}_{12} = \{s_4, s_6\}$. We treat the London transportation network as bidirectional, thus $\mathcal{P}_{ij} \equiv \mathcal{P}_{ji}$. Of note, stations on the paths *do not* necessarily belong to $\{s_1, \dots, s_n\}$.

Now consider the station s_i . For all other stations under study, we have a list of (shortest) paths involving s_i , namely $\{\mathcal{P}_{iu}\}_{u \neq i}$. Similarly, we have the list of paths $\{\mathcal{P}_{jv}\}_{v \neq j}$. Now for any pair (u, v) that is not (j, i) , we can explore if $\mathcal{P}_{iu} \cap \mathcal{P}_{jv} = \emptyset$. If not, then passengers going from i to u and passengers going from j to v are traveling on overlapped routes. We then compute the following quantity

$$k_{ij}^\alpha k_{ji}^{1-\alpha} + \sum_{u \notin \{i, j\}} \sum_{v \notin \{i, j\}} I_{\{\mathcal{P}_{iu} \cap \mathcal{P}_{jv} \neq \emptyset\}} k_{iu}^\alpha k_{jv}^{1-\alpha},$$

where k_{ij} is the fraction of workforce in borough i that goes to borough j for work. The parameter α is for aggregating workforce measures.

We compute shortest paths between stations using London tube network data (station nodes and links between stations) source from <https://github.com/nicola/tubemaps/tree/master/datasets>. Shortest paths are calculated using the Dijkstra's algorithm. Since we do not have complete London transportation network data (bus, overground and train in addition to the tube), our co-traveling network construction is limited. For example, there are six London boroughs (Bexley, Bromley, Croydon, Kingston upon Thames, Lewisham, and Sutton) that do not have tube access at all. We exclude them from our analysis here. Figure A1 visualise the co-traveling network constructed under $\alpha = 0.5$.

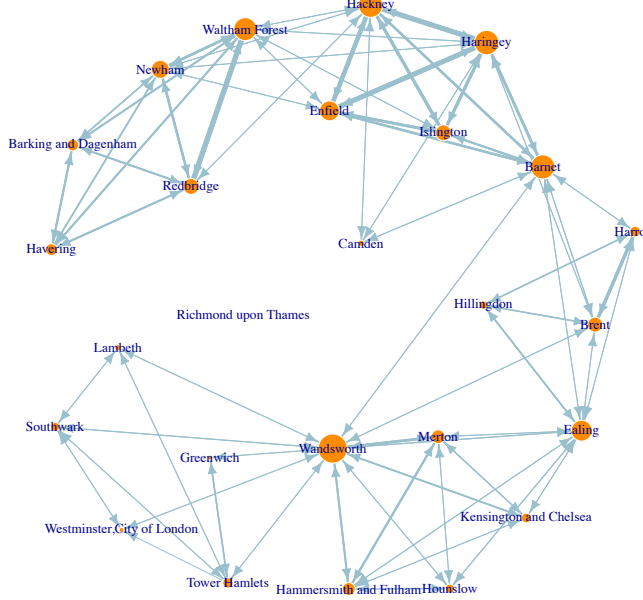


Figure A1: The graph of co-traveling network. Nodes represent London boroughs. Node sizes are proportional to their total in-degrees. Edge widths are proportional to their respective values in the graph. Only edges which exceed the 80% percentile are drawn.

We tabulate the estimation results of including only the co-traveling network, adding the co-traveling network (network “c”) to the work-to-home (network “1”) and home-to-work networks (network “2”), as well as only including the the work-to-home and home-to-work networks in Table A2. Of note, the data here only cover 26 boroughs (excluding ones that are not accessible directly within the tube network). Our construction of co-traveling network based on London underground does show large impacts on the network effects ($\exp(\phi_0^{(3)}) = 1$), either analyzed along or adjusted by our two commuting networks. However, we do not have enough power to reject that $\exp(\phi_0^{(3)}) = 0$. The parameter estimates based on the 26 boroughs under model $\mathcal{G} = (1, 2)$ is close to the full sample estimates reported in Table 1, thus our main estimates are largely unaffected by the inclusion of co-traveling network.

Table A2: The effects of co-traveling network.

Model \mathcal{G}	(c)		(1,2,c)		(1,2)	
Value	est.	se.	est.	se.	est.	se.
Autoregressive effect						
$\exp(\gamma_0)$	0.667	0.017	0.342	0.039	0.343	0.039
$\exp(\gamma)$	0.332	0.020	0.517	0.069	0.502	0.067
Network effect						
$W^{(1)} = K$:						
$\exp(\phi_0^{(1)})$			0.580	0.113	0.599	0.076
$\exp(\phi^{(1)})$			0.421	0.177	0.636	0.107
$W^{(2)} = K^\top$:						
$\exp(\phi_0^{(2)})$			0.051	0.023	0.046	0.023
$\exp(\phi^{(2)})$			0.890	0.426	0.278	0.439
$W^{(c)}$ (co-traveling network):						
$\exp(\phi_0^{(3)})$	1.000	0.781	1.000	6.118		
$\exp(\phi^{(3)})$	1.000	2.661	1.000	7.692		
pseudo- R^2	82.3%		82.8%		82.9%	
# obs.	2444		2444		2444	

E Additional Tables

Table A3: Estimation results of the Network-SIR model of Section 1.3. All five models under consideration include only the first two networks. The decaying kernel function $v(\ell) = \exp(-\rho\ell)$ controls the temporal dependence structure of the infected cases across boroughs. Parameter estimates under five values of ρ (0.4, 0.6, 0.8, 1, 1.2) around the optimal value 0.8 (maximising the profiled likelihood function) are reported.

ρ Value	$\rho = 0.4$		$\rho = 0.6$		$\rho = 0.8$		$\rho = 1$		$\rho = 1.2$	
	est.	se.	est.	se.	est.	se.	est.	se.	est.	se.
Autoregressive effect										
$\exp(\gamma_0)$	0.186	0.026	0.307	0.031	0.341	0.037	0.361	0.043	0.371	0.048
$\exp(\gamma)$	0.999	0.143	0.525	0.060	0.522	0.065	0.517	0.070	0.528	0.076
Network effect										
$\mathbf{W}^{(1)} = K:$										
$\exp\left(\phi_0^{(1)}\right)$	0.264	0.045	0.479	0.055	0.582	0.069	0.685	0.082	0.771	0.093
$\exp\left(\phi^{(1)}\right)$	0.657	0.113	0.600	0.084	0.636	0.102	0.768	0.107	0.602	0.093
$\mathbf{W}^{(2)} = K^\top:$										
$\exp\left(\phi_0^{(2)}\right)$	0.027	0.014	0.027	0.017	0.039	0.020	0.049	0.023	0.067	0.025
$\exp\left(\phi^{(2)}\right)$	0.003	0.087	0.000	0.000	0.182	0.427	0.028	0.395	0.696	0.272
pseudo- R^2	82.0%		81.9%		81.9%		81.9%		81.9%	
$\log L$	−7390.2		−7327.3		−7315.9		−7326.8		−7339.8	
# obs.	3008		3008		3008		3008		3008	

Table A4: Estimation results of the Network-SIR model of Section 1.3. Results in columns (1)-(3) correspond, respectively, to specifications with only one of the following transmission networks: “work-to-home”, “home-to-work”, and “home-to-home”. Column (1,2,3) include all the three networks while column (1,2) uses only the first two networks. Test-related variables are included into the endemic terms.

Model \mathcal{G}	(1)		(2)		(3)		(1,2,3)		(1,2)	
Value	est.	se.	est.	se.	est.	se.	est.	se.	est.	se.
Autoregressive effect										
$\exp(\gamma_0)$	0.313	0.035	0.286	0.040	0.286	0.037	0.254	0.041	0.252	0.041
$\exp(\gamma)$	0.607	0.075	0.958	0.136	0.749	0.102	0.752	0.127	0.760	0.129
Network effect										
$\mathbf{W}^{(1)} = K:$										
$\exp\left(\phi_0^{(1)}\right)$	0.489	0.066					0.510	0.073	0.503	0.075
$\exp\left(\phi^{(1)}\right)$	0.896	0.132					0.827	0.127	0.821	0.129
$\mathbf{W}^{(2)} = K^\top:$										
$\exp\left(\phi_0^{(2)}\right)$			0.115	0.022			0.064	0.023	0.062	0.023
$\exp\left(\phi^{(2)}\right)$			0.374	0.080			0.169	0.181	0.149	0.187
$\exp\left(\phi_0^{(3)}\right)$					0.262	0.035	0.000	0.000		
$\exp\left(\phi^{(3)}\right)$					0.570	0.082	0.042	0.000		
Testing-related endemic effect										
pos-to-test	-1.36	0.48	-1.09	0.28	-1.46	0.41	-1.46	0.49	-1.46	0.48
lag test	1.84	0.32	1.77	0.23	1.88	0.28	1.91	0.32	1.91	0.31
pseudo- R^2	82.1%		82.0%		82.0%		82.1%		82.1%	
# obs.	3008		3008		3008		3008		3008	

Table A5: Estimation results of the Network-SIR model of Section 1.3 adding week fixed effects. Results in columns (1)-(3) correspond, respectively, to specifications with only one of the following transmission networks: “work-to-home;” “home-to-work;” “home-to-home”. Column (1,2,3) considers the three networks jointly while column (1,2) uses only the first two networks.

Model \mathcal{G}	(1)		(2)		(3)		(1,2,3)		(1,2)	
Value	est.	se.	est.	se.	est.	se.	est.	se.	est.	se.
Autoregressive effect										
$\exp(\gamma_0)$	0.313	0.031	0.333	0.026	0.283	0.032	0.266	0.033	0.269	0.033
$\exp(\gamma)$	0.604	0.072	0.649	0.051	0.695	0.091	0.702	0.100	0.701	0.100
Network effect										
$\mathbf{W}^{(1)} = K$										
$\exp\left(\phi_0^{(1)}\right)$	0.375	0.055					0.342	0.131	0.378	0.057
$\exp\left(\phi^{(1)}\right)$	0.832	0.160					0.733	0.382	0.822	0.161
$\mathbf{W}^{(2)} = K^\top$										
$\exp\left(\phi_0^{(2)}\right)$			0.101	0.035			0.070	0.041	0.071	0.028
$\exp\left(\phi^{(2)}\right)$			0.160	0.186			0.000	0.000	0.000	0.000
$\mathbf{W}^{(3)} = KK^\top$										
$\exp\left(\phi_0^{(3)}\right)$					0.243	0.036	0.035	0.097		
$\exp\left(\phi^{(3)}\right)$					0.459	0.098	1.000	2.860		
pseudo- R^2	81.2%		81.1%		81.1%		81.2%		81.2%	
# obs.	3008		3008		3008		3008		3008	

Table A6: Sensitivity analysis of the Network-SIR model of Section 1.3. Results in columns (1)-(3) correspond, respectively, to specifications with only one of the following transmission networks: “work-to-home;” “home-to-work;” “home-to-home”. Column (1,2,3) considers the three networks jointly while column (1,2) uses only the first two networks.

Model \mathcal{G} Value	(1)		(2)		(3)		(1,2,3)		(1,2)	
	est.	se.	est.	se.	est.	se.	est.	se.	est.	se.
Autoregressive effect										
$\exp(\gamma_0)$	0.402	0.045	0.511	0.045	0.429	0.057	0.359	0.061	0.363	0.062
$\exp(\gamma) : 3.17 - 3.20$	1.000	0.216	1.000	0.088	1.000	0.179	1.000	0.285	1.000	0.267
$\exp(\gamma) : 3.21 - 3.23$	0.814	0.217	0.288	0.115	0.910	0.174	0.813	0.320	0.809	0.279
$\exp(\gamma) : 3.24 - 6.03$	0.444	0.056	0.454	0.045	0.445	0.064	0.522	0.094	0.492	0.089
Network effect										
$\mathbf{W}^{(1)} = K:$										
$\exp(\phi_0^{(1)})$	0.546	0.083					0.508	0.332	0.578	0.096
$\exp(\phi^{(1)}) : 3.17 - 3.20$	1.000	0.314					1.000	0.942	1.000	0.308
$\exp(\phi^{(1)}) : 3.21 - 3.23$	1.000	0.332					1.000	1.197	1.000	0.388
$\exp(\phi^{(1)}) : 3.24 - 6.03$	0.697	0.120					0.782	0.525	0.642	0.127
$\mathbf{W}^{(2)} = K^\top:$										
$\exp(\phi_0^{(2)})$			0.122	0.042			0.053	0.081	0.064	0.036
$\exp(\phi^{(2)}) : 3.17 - 3.20$			0.285	0.319			0.138	1.283	0.374	0.650
$\exp(\phi^{(2)}) : 3.21 - 3.23$			1.000	0.447			0.526	1.974	0.555	1.000
$\exp(\phi^{(2)}) : 3.24 - 6.03$			0.367	0.132			0.000	0.000	0.095	0.261
$\mathbf{W}^{(3)} = KK^\top:$										
$\exp(\phi_0^{(3)})$					0.317	0.064	0.054	0.260		
$\exp(\phi^{(3)}) : 3.17 - 3.20$					0.906	0.259	1.000	5.728		
$\exp(\phi^{(3)}) : 3.21 - 3.23$					0.704	0.229	1.000	6.421		
$\exp(\phi^{(3)}) : 3.24 - 6.03$					0.514	0.107	1.000	4.867		
pseudo- R^2	81.9%		81.3%		81.6%		81.5%		81.9%	
# obs.	3008		3008		3008		3008		3008	

Table A7: Changes in activities from Google after the March 23 lockdown in Each London Borough

Borough	Activity reduction: workplaces
Barking and Dagenham	54.2%
Barnet	62.3%
Bexley	57.3%
Brent	59.2%
Bromley	63.2%
Camden	68.4%
Croydon	58.9%
Ealing	60.7%
Enfield	55.8%
Greenwich	60.4%
Hackney	62.3%
Hammersmith and Fulham	68.1%
Haringey	63.7%
Harrow	59.9%
Havering	57.3%
Hillingdon	58.9%
Hounslow	60.2%
Islington	67.9%
Kensington and Chelsea	66.2%
Kingston upon Thames	64.6%
Lambeth	65.4%
Lewisham	63.5%
Merton	61.8%
Newham	61.7%
Redbridge	61.4%
Richmond upon Thames	67.7%
Southwark	65.1%
Sutton	58.7%
Tower Hamlets	69.6%
Waltham Forest	61.9%
Wandsworth	67.8%
Westminster, City of London	58.6%